

Asymptotically flat hairy black holes in massive bigravity

Romain Gervalle^{1,*} and Mikhail S. Volkov^{1,2,3,†}

¹*Institut Denis Poisson, UMR - CNRS 7013,*

Université de Tours, Parc de Grandmont, 37200 Tours, France

²*Institute for Theoretical and Mathematical Physics,*

Lomonosov Moscow State University, Leninskie Gory, GSP-1, 119991 Moscow, Russia

³*Department of General Relativity and Gravitation, Institute of Physics,*

Kazan Federal University, Kremlevskaya street 18, 420008 Kazan, Russia

We study asymptotically flat black holes with massive graviton hair within the ghost-free bigravity theory. There have been contradictory statements in the literature about their existence – such solutions were reported some time ago, but later a different group claimed the Schwarzschild solution to be the only asymptotically flat black hole in the theory. As a result, the controversy emerged. We have analysed the issue ourselves and have been able to construct such solutions within a carefully designed numerical scheme. We find that for given parameter values there can be one or two asymptotically flat hairy black holes in addition to the Schwarzschild solution. We analyze their perturbative stability and find that they can be stable or unstable, depending on the parameter values. The stable hairy black holes that would be physically relevant can be neither very small nor very large and always have the mass and size close to those for the ordinary black holes of mass $M \sim 10^6 M_\odot$. One of their two geometries is very close to Schwarzschild. If the bigravity theory indeed describes physics, this would imply that the supermassive astrophysical black holes hide inside the “hairy features” that should manifest themselves in violent processes like black hole collisions.

* romain.gervalle@univ-tours.fr

† volkov@lmpt.univ-tours.fr

I. Introduction

Theories with massive gravitons provide a natural modification of the General Relativity (GR) in the infrared regime and can be used to explain the current acceleration of our Universe [1, 2]. Such theories have a long history pioneered by the work of by Fierz and Pauli [3] and marked by subsequent discoveries of many interesting features, such as the vDVZ discontinuity [4, 5], the Vainshtein mechanism [6], the Boulware-Deser ghost [7], culminating in the discovery of the ghost-free massive gravity [8] and ghost-free bigravity [9] theories.

The ghost-free bigravity theory is the most interesting physically. It contains two dynamical metrics, usually called $g_{\mu\nu}$ and $f_{\mu\nu}$, describing together two gravitons, one of which is massive and the other is massless. The theory admits self-accelerating cosmological solutions [10–12] whose properties agree with the observations [13–17], with the Λ -term mimicked by the graviton mass. The theory also admits solutions describing black holes [18], wormholes [19], and other interesting solutions (see [20] for a review). In what follows we shall be discussing black holes.

The bigravity black holes can be either “bald” or “hairy”. The bald black holes are described by the known GR metrics. Such solutions were first discovered long ago [21–23] within the old bigravity theory inspired by physics of strong interactions [24]. In the simplest case, their two metrics are both Schwarzschild-(anti)-de Sitter and can be conveniently represented in the Eddington-Finkelstein coordinates as [25, 26]

$$g_{\mu\nu}dx^\mu dx^\nu = -\Sigma_g dv^2 + 2dvdr + r^2 d\Omega^2, \quad f_{\mu\nu}dx^\mu dx^\nu = C^2 \left(-\Sigma_f dv^2 + 2dvdr + r^2 d\Omega^2 \right), \quad (1.1)$$

with $\Sigma_g = 1 - 2M_g/r + \Lambda_g/(3r^2)$ and $\Sigma_f = 1 - 2M_f/r + \Lambda_f/(3r^2)$, where values of constants C, Λ_g, Λ_f are fixed by the field equations. Passing to the Schwarzschild coordinates, one can diagonalize one of the two metrics, but not both of them simultaneously. Such solutions have been much studied [27], they exist also within the ghost-free bigravity [28], and they admit the charged [29] and spinning [30] generalizations. These solutions also admit the massive gravity limit where $M_f = \Lambda_f = 0$ hence the f-metric is flat while the g-metric remains non-trivial, and this yields all possible static black holes in the ghost-free massive gravity theory (it seems there can be also time-dependent black holes in this theory [31]).

Next, it was noticed in [18] that if the parameters of the potential are suitably adjusted, then the ghost-free bigravity reduces to the vacuum GR in the sector where the two metrics coincide, $g_{\mu\nu} = f_{\mu\nu}$. Therefore, all vacuum GR black holes, as for example the Schwarzschild

solution,

$$g_{\mu\nu}dx^\mu dx^\nu = f_{\mu\nu}dx^\mu dx^\nu = -\left(1 - \frac{2M}{r}\right) dt^2 + \frac{dr^2}{1 - 2M/r} + r^2 d\Omega^2, \quad (1.2)$$

or its spinning generalization can be imbedded into the ghost-free bigravity. A Λ -term can be included by assuming the two metrics to be proportional to each other [18, 20, 26]. Such solutions are different from solutions of type (1.1), for example they do not admit the massive gravity limit. In addition, the solution (1.1) is linearly stable [32], whereas the solution (1.2) is unstable with respect to fluctuations which do not respect the condition $g_{\mu\nu} = f_{\mu\nu}$ [33].

These facts essentially exhaust the available knowledge of the “bald” black holes in the bigravity theory. At the same time, more general “hairy” black holes not described by the classical GR metrics can exist as well. The first example of hairy black holes in physics was found long ago [34], followed by many other examples (see [35, 36] for a review), so that nowadays hairy black holes are considered as something usual. One may therefore wonder if they exist in the ghost-free bigravity theory as well.

A systematic analysis of hairy black holes in the ghost-free massive bigravity has been carried out for the first time by one of the authors [18], but none of the solutions found were asymptotically flat. In that analysis both metrics were assumed to be static and spherically symmetric. If they are not simultaneously diagonal, then the most general solution is given by (1.1). If they are simultaneously diagonal, then one of the solutions is given by (1.2), but other more general black hole solutions exist as well.

Such solutions possess an event horizon – a hypersurface that is null simultaneously with respect to $g_{\mu\nu}$ and $f_{\mu\nu}$. Therefore, both metrics share the horizon [37, 38], but its radius r_H^g measured by $g_{\mu\nu}$ can be different from the radius r_H^f measured by $f_{\mu\nu}$. One can set $r_H \equiv r_H^g$ to unit value via rescaling the system (rescaling at the same time the graviton mass), but the ratio $u = r_H^g/r_H^f$ is scale-invariant. Choosing a value of u completely determines the boundary conditions at the horizon, which allows one to integrate the equations starting from the horizon toward large values of the radial coordinate r . As a result, the set of all black hole solutions can be labeled by just one parameter u , and integrating the equations for different values of u gives all possible black holes.

Choosing $u = 1$ yields the Schwarzschild solution (1.2). For $u \neq 1$ one finds more general black holes supporting a massive graviton “hair” outside the horizon, but in the asymptotic region their two geometries do not become flat [18]. The latter property is generic, and trying different values of u always gives either solutions with a curvature singularity somewhere outside the horizon, or solutions which exist for all values of r but show non-flat asymptotics.

At the same time, these facts do not completely exclude a possibility of some other asymp-

totically flat black hole solutions different from (1.2) which would correspond to some special values of u different from $u = 1$. However, even if they exist, one does not find them by a brute force via trying many different values of u , and the reason is the following. The field equations reduce to three coupled first order ODE's [18], whose *local* at large r solution which approaches flat geometry as $r \rightarrow \infty$ has schematically the following structure (A, B, C being integration constants):

$$\frac{A}{r} + Be^{-r} + Ce^{+r}. \quad (1.3)$$

Here $r = mr$ is the dimensionless radial coordinate, with m and r being the graviton mass and dimensionful radial coordinate (we assume the graviton mass to have the dimension of inverse length, so that this is rather the inverse Compton wavelength mc/\hbar). The Newtonian mode A/r in (1.3) arises due to the massless graviton present in the theory, while the decaying mode Be^{-r} and the growing mode Ce^{+r} are due to the massive graviton. Now, when integrating from the horizon, the growing mode Ce^{+r} will be inevitably present in the numerical solution at large r and will drive the solution away from flat space. This is why one does not find asymptotically flat solutions in this way.

To get them, one should suppress the growing mode by setting $C = 0$, hence the local solutions at large r will comprise a two-parameter set labeled by A and B . The next step is to numerically extend this local solution toward small r , extending at the same time the local solution at the horizon labeled by u toward large r , until the two solutions meet at some intermediate point. For these solutions to agree, three (the number of the ODE's) matching conditions should be satisfied via adjusting the three parameters u, A, B . In practice, this can be done within the numerical multiple-shooting method [39]. Once u, A, B are adjusted, this yields global asymptotically flat solutions.

The difficulty, however, is that the numerical scheme requires some input values of u, A, B which should be close to the “true values”, otherwise the iterations do not converge. It was apriori unclear how to choose these input values, whereas choosing them randomly does not give the convergence. Some additional information was needed to properly choose these values, but at the time of writing the article [18] such an information was not available. As a result, the conclusion of that work was that asymptotically flat hairy black holes may exist, but they should be parametrically isolated from the Schwarzschild solution (1.2).

It is interesting that adding an extra matter source to obtain not a black hole but a regular object like a star, asymptotically flat solutions can be easily constructed, as was shown first in [18] and later in [40, 41]. The black hole case is more difficult.

Fortunately, the additional information was later obtained within the analysis of pertur-

bations of the Schwarzschild solution (1.2) [33, 42]. Denoting $g_{\mu\nu}^S$ the Schwarzschild metric, the two perturbed metrics are $g_{\mu\nu} = g_{\mu\nu}^S + \delta g_{\mu\nu}$ and $f_{\mu\nu} = g_{\mu\nu}^S + \delta f_{\mu\nu}$. Linearizing the field equations with respect to $\delta g_{\mu\nu}$ and $\delta f_{\mu\nu}$, one finds that perturbations grow in time and hence the background Schwarzschild black hole is unstable if $r_H \equiv mr_H \leq 0.86$. On the other hand, for $r_H > 0.86$ the perturbations are bounded in time so that the background is stable [33]. Curiously, the mathematical structure of the perturbation equations is identical [33] to that previously discovered by Gregory and Laflamme (GL) in their analysis of black strings in D=5 GR [43]. We shall therefore refer to the Schwarzschild solution with $r_H = 0.86$ as GL point.

This change of stability at the GL point suggests that for r_H close to 0.86 there could be two different asymptotically flat solutions: the Schwarzschild solution (1.2) and also some other solution which can be approximated by the zero perturbation mode that exists at the GL point. This new solution is different from Schwarzschild although close to it, hence it describes an asymptotically flat hairy black hole. To get this solution within the numerical scheme outlined above, one should choose the input parameters u, A, B to be close the GL point, $u \approx 1$, $r_H \approx 0.86$, $A \approx -r_H/2$, $B \approx 0$, and it is this essential piece of information that was missing when writing Ref.[18]. As soon as the solution is obtained, one can change the value of r_H iteratively, thus obtaining “fully fledged” hairy black holes which may deviate considerably from the parent Schwarzschild solution.

Remarkably, this program was accomplished by the Portuguese group [44] via explicitly constructing asymptotically flat hairy black holes in the theory in the region *below* the GL point, for $r_H < 0.86$. However, some time later spherically symmetric bigravity solutions were analyzed by the Swedish group [45], and it was claimed that the Schwarzschild solution (1.2) represents the unique asymptotically flat black hole in the theory. As a result, a controversy emerged and it was unclear if asymptotically flat hairy black holes exist or not.

We have therefore reconsidered the issue ourselves and below are our results. In brief, we were able to construct asymptotically flat hairy black holes in the theory, thereby confirming the finding of [44]. We apply a very carefully designed numerical scheme to exclude any ambiguities and to take into account the arguments of [45]. In fact, these arguments correctly point to some drawbacks of numerical analysis commonly present in many publications. From the mathematical viewpoint, one has to solve a non-linear boundary value problem where the boundaries are singular points of the differential equations (horizon and infinity). Since it is difficult to approach such points numerically, various approximations are used in practice, which may give reasonable results in some cases but inevitably increases the error and leads to a numerical instability. Only very rarely does one find in the literature a correct treatment

of the problem (apart from the relaxation approach), as for example in [46–48]. We therefore pay a special attention to the details of our numerical scheme and describe them in a very explicit way. As a result, from the methodological viewpoint, our paper gives an example of how one should properly tackle a non-linear boundary value problem with singular endpoints.

We cross-check our results with two different numerical codes written independently by two of us. Our results strongly suggest that the hairy solutions exist and are indeed asymptotically flat and regular. We discover many of their new features, in particular we obtain hairy black holes also *above* the GL point for $r_H > 0.86$, and we study for the first time the perturbative stability of the solutions. We were able to identify regions in the parameter space which correspond to stable solutions, and we determined subsets of these regions which agree with the constraints imposed by the cosmological observations. We find that the viable hairy black holes should be described by the g-metric that is very close to Schwarzschild, but their f-metric is different. The mass and size of these black holes should be close to those for the usual black holes of mass $M \sim 10^6 M_\odot$. Therefore, if the bigravity theory indeed describes physics, the supermassive astrophysical black holes should hide inside the “hairy features”.

We have also attentively considered the arguments of Ref. [45]. In brief, this work seems to agree that the solutions exist but judges them physically unacceptable. We analyse the arguments and we think some of them are interesting and should be taken into consideration, but none of them is decisive, so that they should rather be viewed as a conjecture. To understand its origin, we notice that the numerical procedure adopted in that work is not suitable for suppressing the growing at infinity mode, which generates artificial numerical singularities. This must be reason why the solutions were judged unacceptable in that work. However, no singularities appear within the properly chosen numerical scheme, and we specially adapt our scheme to be able to cope with the arguments of [45]. We shall postpone a more detailed discussion of Ref. [45] until the end of this text to be able to make a comparison with our results.

The rest of the text is organized as follows. In Section II we introduce the massive bigravity theory of Hassan and Rosen [9]. The field equations, their reduction to the static and spherically symmetric sector, and the simplest solutions are described in Sections III–V. In Sections VI, VII we describe in detail our analysis of boundary conditions at the horizon and at infinity, and then summarize in Section VIII the structure of our numerical procedure. In Section IX we show our solutions for asymptotically flat hairy black holes and also describe the duality relation yielding the solutions above the GL point. After that, we discuss in Section X the perturbations of the hairy backgrounds and the analysis of the negative perturbation modes.

Our discussion culminates in Section XI where we describe various limits and identify regions in the parameter space where the solutions exist and where they are stable. In Section XII we give a brief summary of our results and discuss the arguments of Ref.[45]. The two Appendices contain the description of the desingularization of the equations at the horizon, as well as the complete set of the field equations in the time-dependent case.

II. The ghost-free bigravity

The theory is defined on a four-dimensional spacetime manifold endowed with two Lorentzian metrics $g_{\mu\nu}$ and $f_{\mu\nu}$ with the signature $(-, +, +, +)$. The action is [9]

$$S[g, f] = \frac{1}{2\kappa_1} \int R(g) \sqrt{-g} d^4x + \frac{1}{2\kappa_2} \int R(f) \sqrt{-f} d^4x - \frac{m^2}{\kappa} \int \mathcal{U} \sqrt{-g} d^4x, \quad (2.1)$$

where κ_1 and κ_2 are the gravitational couplings, κ is a parameter with the same dimension, and m is a mass parameter. The interaction between the two metrics is expressed by a scalar function of the tensor (the hat denotes matrices)

$$\hat{\gamma} = \sqrt{\hat{g}^{-1}\hat{f}}. \quad (2.2)$$

Here the matrix square root is understood in the sense that $\hat{\gamma}^2 = \hat{g}^{-1}\hat{f}$, which can be written in components as

$$(\gamma^2)^\mu{}_\nu \equiv \gamma^\mu{}_\alpha \gamma^\alpha{}_\nu = g^{\mu\alpha} f_{\alpha\nu}. \quad (2.3)$$

If λ_a ($a = 1, 2, 3, 4$) are the eigenvalues of $\gamma^\mu{}_\nu$ then the interaction potential is

$$\mathcal{U} = \sum_{n=0}^4 b_n \mathcal{U}_n, \quad (2.4)$$

where b_k are dimensionless parameters while \mathcal{U}_k are defined by the relations

$$\begin{aligned} \mathcal{U}_0 &= 1, \quad \mathcal{U}_1 = \sum_a \lambda_a = [\gamma], \\ \mathcal{U}_2 &= \sum_{a<b} \lambda_a \lambda_b = \frac{1}{2!} ([\gamma]^2 - [\gamma^2]), \\ \mathcal{U}_3 &= \sum_{a<b<c} \lambda_a \lambda_b \lambda_c = \frac{1}{3!} ([\gamma]^3 - 3[\gamma][\gamma^2] + 2[\gamma^3]), \\ \mathcal{U}_4 &= \lambda_1 \lambda_2 \lambda_3 \lambda_4 = \det(\hat{\gamma}). \end{aligned}$$

Here $[\gamma] = \text{tr}(\hat{\gamma}) \equiv \gamma^\mu{}_\mu$ and $[\gamma^k] = \text{tr}(\hat{\gamma}^k) \equiv (\gamma^k)^\mu{}_\mu$. The two metrics actually enter the action in a completely symmetric way, since the action is invariant under

$$g_{\mu\nu} \leftrightarrow f_{\mu\nu}, \quad \kappa_1 \leftrightarrow \kappa_2, \quad b_k \leftrightarrow b_{4-k}. \quad (2.5)$$

The action is also invariant under rescalings $\kappa \rightarrow \pm\lambda^2\kappa$, $b_k \rightarrow \pm b_k$, $m \rightarrow \lambda m$, and this allows one to impose, without any loss of generality, the normalization condition $\kappa = \kappa_1 + \kappa_2$. Varying the action with respect to the two metrics gives two sets of Einstein equations,

$$G_{\mu\nu}(g) = m^2 \kappa_1 T_{\mu\nu}, \quad G_{\mu\nu}(f) = m^2 \kappa_2 \mathcal{T}_{\mu\nu}, \quad (2.6)$$

where $\kappa_1 \equiv \kappa_1/\kappa$ and $\kappa_2 \equiv \kappa_2/\kappa$, and the normalization of κ implies that $\kappa_1 + \kappa_2 = 1$. The source terms in (2.6) are obtained by varying the interaction potential \mathcal{U} ,

$$T^\mu_\nu = g^{\mu\alpha} T_{\alpha\nu} = \tau^\mu_\nu - \mathcal{U} \delta^\mu_\nu, \quad \mathcal{T}^\mu_\nu = f^{\mu\alpha} \mathcal{T}_{\alpha\nu} = -\frac{\sqrt{-g}}{\sqrt{-f}} \tau^\mu_\nu, \quad (2.7)$$

where $f^{\mu\alpha}$ is the inverse of $f_{\mu\alpha}$ and

$$\begin{aligned} \tau^\mu_\nu &= \{b_1 \mathcal{U}_0 + b_2 \mathcal{U}_1 + b_3 \mathcal{U}_2 + b_4 \mathcal{U}_3\} \gamma^\mu_\nu \\ &\quad - \{b_2 \mathcal{U}_0 + b_3 \mathcal{U}_1 + b_4 \mathcal{U}_2\} (\gamma^2)^\mu_\nu \\ &\quad + \{b_3 \mathcal{U}_0 + b_4 \mathcal{U}_1\} (\gamma^3)^\mu_\nu - b_4 \mathcal{U}_0 (\gamma^4)^\mu_\nu. \end{aligned} \quad (2.8)$$

There is an identity relation following from the diffeomorphism-invariance of the interaction term in the action,

$$\sqrt{-g} \overset{(g)}{\nabla}_\mu T^\mu_\nu + \sqrt{-f} \overset{(f)}{\nabla}_\mu \mathcal{T}^\mu_\nu \equiv 0, \quad (2.9)$$

where $\overset{(g)}{\nabla}_\rho$ and $\overset{(f)}{\nabla}_\rho$ are the covariant derivatives with respect to $g_{\mu\nu}$ and $f_{\mu\nu}$.

Equations (2.6) describe two interacting gravitons, one massive and one massless. This can be easily seen in the flat space limit. Setting $g_{\mu\nu} = f_{\mu\nu} = \eta_{\mu\nu}$ (the Minkowski metric), Eqs.(2.6) reduce to

$$0 = -m^2 \kappa_1 (P_0 + P_1) \eta_{\mu\nu}, \quad 0 = -m^2 \kappa_2 (P_1 + P_2) \eta_{\mu\nu}, \quad (2.10)$$

with $P_m \equiv b_m + 2b_{m+1} + b_{m+2}$. Therefore, the flat space will be a solution if only the parameters b_k fulfil the conditions $P_1 = -P_0 = -P_2$. Assuming this to be the case, let us set $g_{\mu\nu} = \eta_{\mu\nu} + \delta g_{\mu\nu}$ and $f_{\mu\nu} = \eta_{\mu\nu} + \delta f_{\mu\nu}$ where the deviations $\delta g_{\mu\nu}$ and $\delta f_{\mu\nu}$ are small. Linearizing the equations (2.6) with respect to the deviations yields

$$\hat{\mathcal{E}}_{\mu\nu}^{\alpha\beta} h_{\alpha\beta}^{(0)} = 0, \quad (2.11)$$

$$\hat{\mathcal{E}}_{\mu\nu}^{\alpha\beta} h_{\alpha\beta} + \frac{m_{\text{FP}}^2}{2} (h_{\mu\nu} - \eta_{\mu\nu} h) = 0, \quad (2.12)$$

where $\hat{\mathcal{E}}_{\mu\nu}^{\alpha\beta}$ denotes the linear part of the Einstein operator, and where $h_{\mu\nu}^{(0)} = \kappa_1 \delta f_{\mu\nu} + \kappa_2 \delta g_{\mu\nu}$ and $h_{\mu\nu} = \delta f_{\mu\nu} - \delta g_{\mu\nu}$ with $h = \eta^{\alpha\beta} h_{\alpha\beta}$. The $h_{\mu\nu}^{(0)}$ equations are the linearized Einstein equations describing a massless graviton with two dynamical polarizations. The $h_{\mu\nu}$ field

fulfills the Fierz-Pauli equations for massive gravitons with five polarizations and with the mass

$$m_{\text{FP}}^2 = P_1 m^2. \quad (2.13)$$

Therefore, one will have $m_{\text{FP}} = m$ if

$$P_1 = 1. \quad (2.14)$$

This condition can be solved together with the conditions $P_0 = P_2 = -1$ implied by (2.10) to express the five b_k in terms of two independent parameters, sometimes called c_3 and c_4 ,

$$b_0 = 4c_3 + c_4 - 6, \quad b_1 = 3 - 3c_3 - c_4, \quad b_2 = 2c_3 + c_4 - 1, \quad b_3 = -(c_3 + c_4), \quad b_4 = c_4. \quad (2.15)$$

At the same time, the theory has exactly 7 propagating degrees of freedom also away from the flat space limit and for arbitrary b_k (see [49–51] for its Hamiltonian formulation).

Let us finally pass from the dimensionful spacetime coordinates x^μ to the dimensionless ones,

$$x^\mu = m x^\mu. \quad (2.16)$$

This is equivalent to the conformal rescaling of the metrics,

$$g_{\mu\nu} = \frac{1}{m^2} g_{\mu\nu}, \quad f_{\mu\nu} = \frac{1}{m^2} f_{\mu\nu}, \quad (2.17)$$

after which the field equations (2.6) reduce to

$$G^\mu{}_\nu(g) = \kappa_1 T^\mu{}_\nu, \quad G^\mu{}_\nu(f) = \kappa_2 \mathcal{T}^\mu{}_\nu, \quad (2.18)$$

where $T^\mu{}_\nu$ and $\mathcal{T}^\mu{}_\nu$ are still given by (2.7),(2.8) with $\hat{\gamma} = \sqrt{\hat{g}^{-1}\hat{f}}$. The Bianchi identities for these equations imply that

$$\overset{(g)}{\nabla}_\rho T^\rho{}_\lambda = 0, \quad \overset{(f)}{\nabla}_\rho \mathcal{T}^\rho{}_\lambda = 0, \quad (2.19)$$

which is consistent with (2.9). All fields and coordinates are now dimensionless and no trace of the mass parameter m is left in the equations. However, one has to remember that the unity of length corresponds to the dimensionful $1/m$, which is the physical length scale.

In what follows we shall be analyzing equations (2.18) without making any assumptions about values of κ_1 , κ_2 and b_k . However, when integrating the equations numerically, we shall assume that $\kappa_1 + \kappa_2 = 1$ and choose b_k according to (2.15). Therefore, our solutions depend on three parameters of the theory, c_3, c_4 and η , where

$$\kappa_1 = \cos^2 \eta, \quad \kappa_2 = \sin^2 \eta. \quad (2.20)$$

III. Spherical symmetry

Let us introduce coordinates $(x^0, x^1, x^2, x^3) = (t, r, \vartheta, \varphi)$ and choose both metrics to be static, spherically symmetric, and diagonal,

$$\begin{aligned} ds_g^2 &= g_{\mu\nu} dx^\mu dx^\nu = -Q^2 dt^2 + \frac{dr^2}{\Delta^2} + R^2 d\Omega^2, \\ ds_f^2 &= f_{\mu\nu} dx^\mu dx^\nu = -q^2 dt^2 + \frac{dr^2}{W^2} + U^2 d\Omega^2, \end{aligned} \quad (3.1)$$

where $d\Omega^2 = d\vartheta^2 + \sin^2 \vartheta d\varphi^2$ while Q, Δ, R, q, W, U are functions of the radial coordinate $r = mr$. In fact, this is not the most general form of the spherically symmetric fields, since one could also include the off-diagonal metric element f_{01} as shown by Eq.(B.1) in Appendix B. However, in the *static* case this would imply that (1.1) is the only possible solution [18] (the situation changes in the time-dependent case). Therefore, we choose the static metrics to be both diagonal, which leads to non-trivial solutions.

The tensor γ^μ_ν in (2.2) then reads

$$\gamma^\mu_\nu = \text{diag} \left[\frac{q}{Q}, \frac{\Delta}{W}, \frac{U}{R}, \frac{U}{R} \right], \quad (3.2)$$

and one obtains from (2.7)

$$\begin{aligned} T^\mu_\nu &= \text{diag} [T^0_0, T^1_1, T^2_2, T^2_2], \\ \mathcal{T}^\mu_\nu &= \text{diag} [\mathcal{T}^0_0, \mathcal{T}^1_1, \mathcal{T}^2_2, \mathcal{T}^2_2], \end{aligned} \quad (3.3)$$

where

$$\begin{aligned} T^0_0 &= -\mathcal{P}_0 - \mathcal{P}_1 \frac{\Delta}{W}, \\ T^1_1 &= -\mathcal{P}_0 - \mathcal{P}_1 \frac{q}{Q}, \\ T^2_2 &= -\mathcal{D}_0 - \mathcal{D}_1 \left(\frac{q}{Q} + \frac{\Delta}{W} \right) - \mathcal{D}_2 \frac{q\Delta}{QW}, \\ \mathbf{u}^2 \mathcal{T}^0_0 &= -\mathcal{P}_2 - \mathcal{P}_1 \frac{W}{\Delta}, \\ \mathbf{u}^2 \mathcal{T}^1_1 &= -\mathcal{P}_2 - \mathcal{P}_1 \frac{Q}{q}, \\ \mathbf{u} \mathcal{T}^2_2 &= -\mathcal{D}_3 - \mathcal{D}_2 \left(\frac{Q}{q} + \frac{W}{\Delta} \right) - \mathcal{D}_1 \frac{QW}{q\Delta}. \end{aligned} \quad (3.4)$$

Here $\mathbf{u} = U/R$ and

$$\begin{aligned} \mathcal{P}_m &= b_m + 2b_{m+1}\mathbf{u} + b_{m+2}\mathbf{u}^2, \\ \mathcal{D}_m &= b_m + b_{m+1}\mathbf{u} \quad (m = 0, 1, 2). \end{aligned} \quad (3.5)$$

The independent field equations are

$$\begin{aligned} G_0^0(g) &= \kappa_1 T_0^0, & G_1^1(g) &= \kappa_1 T_1^1, \\ G_0^0(f) &= \kappa_2 \mathcal{T}_0^0, & G_1^1(f) &= \kappa_2 \mathcal{T}_1^1, \end{aligned} \quad (3.6)$$

plus the conservation condition $\overset{(g)}{\nabla}_\mu T_\nu^\mu = 0$, which has only one non-trivial component,

$$\overset{(g)}{\nabla}_\mu T_1^\mu = (T_1^1)' + \frac{Q'}{Q} (T_1^1 - T_0^0) + 2 \frac{R'}{R} (T_1^1 - T_2^2) = 0, \quad (3.7)$$

where the prime denotes differentiation with respect to r . The conservation condition for the second energy-momentum tensor also has only one non-trivial component,

$$\overset{(f)}{\nabla}_\mu \mathcal{T}_1^\mu = (\mathcal{T}_1^1)' + \frac{q'}{q} (\mathcal{T}_1^1 - \mathcal{T}_0^0) + 2 \frac{U'}{U} (\mathcal{T}_1^1 - \mathcal{T}_2^2) = 0, \quad (3.8)$$

but this follows from (3.7) due to the identity relation (2.9). As a result, there are 5 independent equations in (3.6), (3.7), which is enough to determine the 6 field amplitudes Q, Δ, R, q, W, U , because the freedom of reparametrizations of the radial coordinate $r \rightarrow \tilde{r}(r)$ allows one to fix one of the amplitudes.

IV. Field equations

Let us introduce new functions

$$N = \Delta R', \quad Y = W U', \quad (4.1)$$

in terms of which the two metrics read

$$\begin{aligned} ds_g^2 &= -Q^2 dt^2 + \frac{dR^2}{N^2} + R^2 d\Omega^2, \\ ds_f^2 &= -q^2 dt^2 + \frac{dU^2}{Y^2} + U^2 d\Omega^2. \end{aligned} \quad (4.2)$$

The advantage of this parametrization is that the second derivatives disappear from the Einstein tensor and the four Einstein equations (3.6) become

$$N' = -\frac{\kappa_1}{2} \frac{R}{NY} (R'Y\mathcal{P}_0 + U'N\mathcal{P}_1) + \frac{(1-N^2)R'}{2RN}, \quad (4.3)$$

$$Y' = -\frac{\kappa_2}{2} \frac{R^2}{UNY} (R'Y\mathcal{P}_1 + U'N\mathcal{P}_2) + \frac{(1-Y^2)U'}{2UY}, \quad (4.4)$$

$$Q' = -\left(\kappa_1(Q\mathcal{P}_0 + q\mathcal{P}_1) + \frac{Q(N^2-1)}{R^2} \right) \frac{RR'}{2N^2}, \quad (4.5)$$

$$q' = -\left(\kappa_2(Q\mathcal{P}_1 + q\mathcal{P}_2) + \frac{q(Y^2-1)}{R^2} \right) \frac{R^2 U'}{2Y^2 U}. \quad (4.6)$$

The conservation condition (3.7) reads

$$\stackrel{(g)}{\nabla}_\mu T^\mu_1 = \frac{U'}{R} \left(1 - \frac{N}{Y}\right) \left(d\mathcal{P}_0 + \frac{q}{Q} d\mathcal{P}_1\right) + \left(\frac{q'}{Q} - \frac{NQ'U'}{YQR'}\right) \mathcal{P}_1 = 0, \quad (4.7)$$

and using Eqs.(4.5),(4.6), this reduces to

$$R^2 Q \stackrel{(g)}{\nabla}_\mu T^\mu_1 = \frac{U'}{Y} \mathbf{C} = 0, \quad (4.8)$$

where

$$\begin{aligned} \mathbf{C} = & \left(\kappa_2 \frac{R^4 \mathcal{P}_1^2}{2UY} - \kappa_1 \frac{R^3 \mathcal{P}_0 \mathcal{P}_1}{2N} - \frac{(N^2 - 1) R \mathcal{P}_1}{2N} + (N - Y) R d\mathcal{P}_0 \right) Q \\ & + \left(\kappa_2 \frac{R^4 \mathcal{P}_1 \mathcal{P}_2}{2UY} - \kappa_1 \frac{R^3 \mathcal{P}_1^2}{2N} + \frac{(Y^2 - 1) R^2 \mathcal{P}_1}{2UY} + (N - Y) R d\mathcal{P}_1 \right) q, \end{aligned} \quad (4.9)$$

with

$$d\mathcal{P}_m = 2(b_{m+1} + b_{m+2} \mathbf{u}) \quad (m = 0, 1). \quad (4.10)$$

The conservation condition (3.8) becomes

$$-U^2 q \stackrel{(f)}{\nabla}_\mu \mathcal{T}^\mu_1 = \frac{R'}{N} \mathbf{C} = 0. \quad (4.11)$$

The two conditions (4.8) and (4.11) will be fulfilled if $U' = R' = 0$, in which case both metrics are degenerate. If the metrics are not degenerate, then conditions (4.8) and (4.11) reduce to the algebraic constraint

$$\mathbf{C} = 0. \quad (4.12)$$

This constraint can be resolved with respect to q to give

$$q = \Sigma(R, U, N, Y) Q, \quad (4.13)$$

where $\Sigma(N, Y, R, U)$ is the (negative) ratio of the coefficients in front of Q and q in (4.9).

As a result, we obtain four differential equations (4.3)–(4.6) plus one algebraic constraint (4.12). The same equations can be obtained by inserting the metrics (4.2) directly to the action (2.1), which gives

$$S = \frac{4\pi}{m^2 \kappa} \int L dt dr, \quad (4.14)$$

where, dropping a total derivative,

$$\begin{aligned} L = & \frac{1}{\kappa_1} \left(\frac{(1 - N^2) R'}{N} - 2RN' \right) Q + \frac{1}{\kappa_2} \left(\frac{(1 - Y^2) U'}{Y} - 2UY' \right) q \\ & - \frac{QR^2 R'}{N} \mathcal{P}_0 - \left(\frac{QR^2 U'}{Y} + \frac{qR^2 R'}{N} \right) \mathcal{P}_1 - \frac{qR^2 U'}{Y} \mathcal{P}_2. \end{aligned} \quad (4.15)$$

Varying L with respect to N, Y, Q, q gives Eqs.(4.3)–(4.6), while varying it with respect to R, U reproduces conditions (4.8) and (4.11). The equations and the Lagrangian L are invariant under the interchange symmetry (2.5), which now reads

$$\kappa_1 \leftrightarrow \kappa_2, \quad Q \leftrightarrow q, \quad N \leftrightarrow Y, \quad R \leftrightarrow U, \quad b_m \leftrightarrow b_{4-m}. \quad (4.16)$$

Equation (4.3)–(4.6) contain R' and U' which are not yet known. One of these two amplitudes can be fixed by imposing a gauge condition, but the other one should be determined dynamically. We need therefore one more condition, and the only way to get it is to differentiate the constraint. Since the constraint should be stable, this gives the secondary constraint:

$$\mathbf{C}' = \frac{\partial \mathbf{C}}{\partial N} N' + \frac{\partial \mathbf{C}}{\partial Y} Y' + \frac{\partial \mathbf{C}}{\partial Q} Q' + \frac{\partial \mathbf{C}}{\partial q} q' + \frac{\partial \mathbf{C}}{\partial R} R' + \frac{\partial \mathbf{C}}{\partial U} U' = 0. \quad (4.17)$$

Expressing here the derivatives N', Y', Q', q' by Eqs.(4.3)–(4.6) and using the relation (4.13), this condition reduces to

$$\mathbf{C}' = \mathcal{A}(R, U, N, Y) R' + \mathcal{B}(R, U, N, Y) U' = 0, \quad (4.18)$$

where the functions $\mathcal{A}(R, U, N, Y)$ and $\mathcal{B}(R, U, N, Y)$ are rather complicated and we do not show them explicitly. When the radial coordinate change, both R' and U' change,

$$r \rightarrow \tilde{r}(r), \quad R' \rightarrow \tilde{R}' = R' \frac{dr}{d\tilde{r}}, \quad U' \rightarrow \tilde{U}' = U' \frac{dr}{d\tilde{r}}, \quad (4.19)$$

but the relation (4.18) between R' and U' remains the same. The secondary constraint can be resolved with respect to U' ,

$$U' = -\frac{\mathcal{A}(R, U, N, Y)}{\mathcal{B}(R, U, N, Y)} R' \equiv \mathcal{D}_U(R, U, N, Y) R'. \quad (4.20)$$

We can now use the gauge symmetry (4.19) to impose the coordinate condition

$$R' = 1 \quad \Rightarrow \quad R = r, \quad (4.21)$$

and then (4.20) reduces to

$$U' = \mathcal{D}_U(r, U, N, Y). \quad (4.22)$$

Now, U' appears in the right-hand sides of Eqs.(4.3) and (4.4), and replacing it there by the value (4.22), these two equations together with (4.22) form a closed system of three equations

$$\begin{aligned} N' &= \mathcal{D}_N(r, U, N, Y), \\ Y' &= \mathcal{D}_Y(r, U, N, Y), \\ U' &= \mathcal{D}_U(r, U, N, Y). \end{aligned} \quad (4.23)$$

The amplitudes Q, q are determined as follows. Injecting (4.13) to (4.5) yields the equation

$$Q' = -\frac{r}{2N^2} \left(\kappa_1(\mathcal{P}_0 + \Sigma(r, U, N, Y)\mathcal{P}_1) + \frac{N^2 - 1}{r^2} \right) Q \equiv \mathcal{F}(r, U, N, Y)Q, \quad (4.24)$$

which determines Q , and when its solution is known, q is determined algebraically from (4.13).

In what follows we shall mainly focus on the three coupled equations (4.23) determining N, Y, U . As soon as their solution is obtained, the amplitudes Q, q are determined from (4.24), (4.13).

V. Analytical solutions

Some simple solutions of the equations can be obtained analytically [18], [52], for which it is convenient to use equation in the form (4.3)–(4.6).

A. Proportional backgrounds

Choosing the two metrics to be conformally related [18], [52],

$$ds_f^2 = C^2 ds_g^2, \quad (5.1)$$

with a constant C , the solution is given by

$$Q^2 = N^2 = Y^2 = 1 - \frac{2M}{r} - \frac{\Lambda(C)}{3} r^2, \quad R = r, \quad q = CQ, \quad U = CR, \quad (5.2)$$

which describes two proportional Schwarzschild-(anti)-de Sitter geometries. The constant C and the cosmological constant $\Lambda(C)$ are determined by

$$\kappa_1(\mathcal{P}_0 + C\mathcal{P}_1) = \frac{\kappa_2}{C}(\mathcal{P}_1 + C\mathcal{P}_2) \equiv \Lambda(C). \quad (5.3)$$

Since \mathcal{P}_m defined by (3.5) are polynomials in $u = U/R = C$, this yields an algebraic equation for C that can have up to four real roots. If the parameters b_k are chosen according to (2.15), then one of the roots is $C = 1$, in which case $\Lambda = 0$.

The value of the dimensionful cosmological constant Λ should agree with the observation, hence one should have

$$\Lambda = m^2 \Lambda \sim 1/R_{\text{Hub}}^2 \quad (5.4)$$

where R_{Hub} is the Hubble radius of our Universe. One way to fulfill this relation is to assume that the graviton mass is extremely small such that the Compton length is of the order of the Hubble radius,

$$1/m \sim R_{\text{Hub}}. \quad (5.5)$$

However, the relation can also be fulfilled by assuming that Λ is very small, which is possible if there is a hierarchy between the two couplings: $\kappa_1 \ll \kappa_2 = 1 - \kappa_1 \sim 1$. Eq.(5.3) implies then that $\Lambda \sim \kappa_1$ and that C should be very close to a root of $\mathcal{P}_1 + C\mathcal{P}_2$. The hierarchy between the two couplings is in fact necessary to reconcile with the observations the perturbation spectrum of the massive bigravity cosmology, for which one should assume that [13–17],

$$\frac{\kappa_1}{\kappa_2} \approx \kappa_1 \sim \left(\frac{M_{\text{ew}}}{M_{\text{Pl}}} \right)^2 \sim 10^{-34} \ll 1, \quad (5.6)$$

where $M_{\text{ew}} \sim 100$ GeV is the electroweak energy scale and $M_{\text{Pl}} \sim 10^{19}$ GeV is the Planck mass. As a result,

$$1/m \sim \sqrt{\Lambda} R_{\text{Hub}} = \sqrt{\kappa_1} R_{\text{Hub}} = \left(\frac{M_{\text{ew}}}{M_{\text{Pl}}} \right) R_{\text{Hub}} \sim 10^6 \text{ km}, \quad (5.7)$$

which is of the order of the solar size. However, in what follows we shall not be always assuming κ_1 to be small and shall present our results for arbitrary $\kappa_1 \in [0, 1]$.

B. Deformed AdS background

Choosing U, q to be constant,

$$U = U_0, \quad q = q_0, \quad (5.8)$$

solves Eqs.(4.6) and (4.8), while Eqs.(4.3)–(4.5) then can be integrated in quadratures [18]. However, such solution is unacceptable, since the f-metric degenerates if $U' = 0$. At the same time, there are other, more general solutions which approach (5.8) for $r \rightarrow \infty$, and for these solutions U' vanishes only asymptotically, hence they are acceptable. The leading at large r terms of such solutions are

$$\begin{aligned} N^2 &= -\kappa_1 \frac{b_0}{3} r^2 - \kappa_1 b_1 U_0 r + \mathcal{O}(1), & Y &= -\frac{\sqrt{3}\kappa_2 b_1}{4U_0 \sqrt{-\kappa_1 b_0}} r^2 + \mathcal{O}(r), \\ Q &= \frac{q_0}{4U_0} r + \mathcal{O}(1), & U &= U_0 + \mathcal{O}\left(\frac{1}{r}\right), & q &= q_0 + \mathcal{O}\left(\frac{1}{r}\right). \end{aligned} \quad (5.9)$$

The g-metric approaches the AdS metric in the leading $\mathcal{O}(r^2)$ order, but the subleading terms do not have the AdS structure.

It turns out that solutions of Eqs.(4.3)–(4.6) generically approach for $r \rightarrow \infty$ either (5.2) or (5.9) (or they show a curvature singularity at a finite r), hence they are not asymptotically flat [18].

VI. Boundary conditions at the horizon

Let us require the g-metric to have a regular event horizon at some $r = r_H$ by demanding the metric components $g_{00} = Q^2$ and $g^{rr} = N^2$ to show simple zeroes at this point. Therefore, we demand that close to this point one has $Q^2 \sim N^2 \sim r - r_H$ and we consider only the exterior region $r \geq r_H$ where $Q^2 > 0$ and $N^2 > 0$. Such a behaviour is compatible with the field equations if only the f-metric also shows a regular horizon at the same place, hence $q^2 \sim Y^2 \sim r - r_H$. As a result, both metrics share a horizon at the same place $r = r_H$, in agreement with [37, 38]. However, the horizon radius measured by the g-metric, r_H , can be different from the radius measured by the second metric, $U(r_H)$. We therefore introduce the parameter $u \equiv \mathbf{u}(r_H) = U(r_H)/r_H$.

As a result, the local solutions close to the horizon are expected to have the form

$$\begin{aligned} N^2 &= \sum_{n \geq 1} a_n (r - r_H)^n, & Y^2 &= \sum_{n \geq 1} b_n (r - r_H)^n, \\ U &= u r_H + \sum_{n \geq 1} c_n (r - r_H)^n, \end{aligned} \quad (6.1)$$

the two other amplitudes being

$$Q^2 = \sum_{n \geq 1} d_n (r - r_H)^n, \quad q^2 = \sum_{n \geq 1} e_n (r - r_H)^n. \quad (6.2)$$

The equations then allow one to recurrently determine the coefficients a_n, b_n, c_n, d_n, e_n . It turns out they all can be expressed in terms of a_1 , which should fulfil a quadratic equation

$$\mathcal{A}a_1^2 + \mathcal{B}a_1 + \mathcal{C} = 0 \quad \Rightarrow \quad a_1 = \frac{1}{2\mathcal{A}} \left(-\mathcal{B} + \sigma \sqrt{\mathcal{B}^2 - 4\mathcal{A}\mathcal{C}} \right), \quad \sigma = \pm 1, \quad (6.3)$$

where $\mathcal{A}, \mathcal{B}, \mathcal{C}$ are functions of u, r_H and of the theory parameters b_k, κ_1, κ_2 . It turns out that one should choose $\sigma = +1$, since choosing $\sigma = -1$ always yields singular solutions. Therefore, for a chosen a value of the horizon size r_H , the local solutions (6.1), (6.2) comprise a set labeled by a continuous parameter u . These local solutions determine the boundary conditions at the horizon, and they can be numerically extended to the region $r > r_H$.

The surface gravity for each metric is [18]

$$\kappa_g^2 = \lim_{r \rightarrow r_H} Q^2 N'^2 = \frac{1}{4} d_1 a_1, \quad \kappa_f^2 = \lim_{r \rightarrow r_H} q^2 \left(\frac{Y}{U'} \right)^2 = \frac{e_1 b_1}{4 c_1^2}, \quad (6.4)$$

and using the values of the expansion coefficients determined by the equations yields the relation $\kappa_g = \kappa_f$, hence the two surface gravities coincide, as coincide the Hawking temperatures,

$$T = \frac{\kappa_g}{2\pi} = \frac{\kappa_f}{2\pi}. \quad (6.5)$$

One has close to the horizon $N(r) \sim Y(r) \sim \sqrt{r - r_H}$ hence the derivatives N' and Y' are not defined at the horizon. The usual practice would then be to start the numerical integration not at $r = r_H$ but at a nearby point $r = r_H + \epsilon$. However, although the dependence on ϵ is expected to be small, still its presence in the procedure may lead to numerical instabilities. This point was emphasised in [45]. This difficulty can be resolved as follows. Setting

$$N(r) = S(r) \nu(r), \quad Y(r) = S(r) y(r) \quad \text{with} \quad S(r) = \sqrt{1 - \frac{r_H}{r}}, \quad (6.6)$$

the functions $\nu(r), y(r)$ and all their derivatives assume finite values at $r = r_H$. Making this change of variables in (4.23) gives a “desingularized” version of the equations that allows us to start the numerical integration exactly at $r = r_H$. This form of the equations is described in Appendix A.

To recapitulate, all black holes for a given r_H can be labeled by only one parameter u . If $u = 1$ then the two metrics coincide everywhere and the solution is Schwarzschild (1.2). If $u = C$ where C is a root of the algebraic equation (5.3), then the solution is Schwarzschild-(anti)-de Sitter and is described by (5.1) and (5.2). For other values of u the numerical integration produces more general solutions which describe hairy black holes and which can be of the following three qualitative types, depending on their asymptotic behaviour [18].

a) Solutions extending up to arbitrarily large values of r and asymptotically approaching a proportional AdS background (5.1), (5.2). At large r one has $N = N_0 (1 + \delta N)$, $Y = Y_0 (1 + \delta Y)$, $U = U_0 (1 + \delta U)$ where N_0, Y_0, U_0 are given by (5.2), while the deviations $\delta N, \delta Y, \delta U$ approach zero. In the linear approximation, the latter are described by

$$\delta N = \frac{A}{r^3}, \quad \delta U = B_1 e^{\lambda_1 r} + B_2 e^{\lambda_2 r}, \quad \delta Y = \mathcal{O}(\delta U), \quad (6.7)$$

where A, B_1, B_2 are integration constants and real parts of λ_1 and λ_2 are *negative*. All of these three perturbation modes vanish for $r \rightarrow \infty$, and since the number of equations (4.23) is also three, it follows that the AdS background is an *attractor* at large r .

b) Solutions extending up to arbitrarily large values of r and asymptotically approaching a deformed AdS background (5.9). The latter is also an attractor at large r .

c) Solutions extending only up to $r = r_s < \infty$ where derivatives of some metric functions diverge, which corresponds to a curvature singularity.

This exhausts the possible types of *generic* solutions. If one integrates the equation for many different values of u , one always obtains solutions of the above three types and one does not find asymptotically flat solutions other than Schwarzschild. For example, choosing $u = 1 + \epsilon$ yields solutions which are almost Schwarzschild in a region close to the horizon,

but for larger values of r they deviate from the Schwarzschild metric more and more [18] (this means the Schwarzschild solution is Lyapunov unstable [45]). All of this does not mean that the Schwarzschild is the only asymptotically flat black hole solution. There may be others, but they are not parametrically close to the Schwarzschild solution and should correspond to some discrete values of u which are difficult to detect by a “brute force” method.

VII. Boundary conditions at infinity

Let us suppose the solutions to approach flat space with $g_{\mu\nu} = f_{\mu\nu} = \eta_{\mu\nu}$ at large r and set

$$N = 1 + \delta N, \quad Y = 1 + \delta Y, \quad U = r + \delta U. \quad (7.1)$$

In fact, a more general possibility would be to require the g-metric to approach the flat Minkowski metric $\text{diag}(-1, 1, 1, 1)$ and the f-metric to approach just a flat metric, as for example $\text{diag}(-a^2, b^2, b^2, b^2)$ with constant a, b . This would lead to solutions whose Lorentz invariance is broken in the asymptotic region [27, 28]. However, we shall not analyze this option.

Inserting (7.1) to (4.23) yields

$$\begin{aligned} \delta N' &= -\frac{1}{r}(\kappa_2 \delta N + \kappa_1 \delta Y) - \kappa_1 \delta U + \mathcal{N}_N, \\ \delta Y' &= -\frac{1}{r}(\kappa_2 \delta N + \kappa_1 \delta Y) + \kappa_2 \delta U + \mathcal{N}_Y, \\ \delta U' &= \left(1 + \frac{2}{r^2}\right) (\delta Y - \delta N) + \mathcal{N}_U, \end{aligned} \quad (7.2)$$

where $\mathcal{N}_N, \mathcal{N}_Y, \mathcal{N}_U$ are the non-linear in $\delta N, \delta Y, \delta U$ parts of the right-hand sides $\mathcal{D}_N, \mathcal{D}_Y, \mathcal{D}_U$ in (4.23). Neglecting the non-linear terms, the solution of these equations is

$$\begin{aligned} \delta N &= \frac{A}{r} + B \kappa_1 \frac{1+r}{r} e^{-r} + C \kappa_1 \frac{1-r}{r} e^{+r}, \\ \delta Y &= \frac{A}{r} - B \kappa_2 \frac{1+r}{r} e^{-r} - C \kappa_2 \frac{1-r}{r} e^{+r}, \\ \delta U &= B \frac{r^2 + r + 1}{r^2} e^{-r} + C \frac{r^2 - r + 1}{r^2} e^{+r}, \end{aligned} \quad (7.3)$$

where A, B, C are integration constants. The part of this solution proportional to A is the Newtonian mode describing the massless graviton subject to the linearized Einstein equations (2.11). The other two modes proportional to B and C fulfill the Fierz-Pauli equations (2.12) and describe the massive graviton, hence they contain the Yukawa exponents (remember that $r = mr$).

As one can see, among the three modes only two are stable for $r \rightarrow \infty$ while the third one diverges in this limit, hence *flat space is not an attractor*. This is why one cannot get

asymptotically flat solutions by simply integrating from the horizon – trying to approach flat space in this way, the unstable mode e^{+r} rapidly wins and drives the solution away from flat space. The only way to proceed is to suppress the unstable mode from the very beginning by requiring the solution at large r to be

$$\begin{aligned}\delta N &= \frac{A}{r} + B \kappa_1 \frac{1+r}{r} e^{-r} + \dots, \\ \delta Y &= \frac{A}{r} - B \kappa_2 \frac{1+r}{r} e^{-r} + \dots, \\ \delta U &= r + B \frac{r^2 + r + 1}{r^2} e^{-r} + \dots,\end{aligned}\tag{7.4}$$

where the dots denote non-linear corrections. The usual practice would be to neglect the dots and assume that the linear terms approximate the solution everywhere for $r > r_*$, where r_* is some large value. However, one can check that already the quadratic correction contains an additional factor of $\ln(r)$ and hence dominates the linear part for $r \rightarrow \infty$. Therefore, non-linear corrections are important, but if all of them are taken into account, it is not obvious that the solution will remain asymptotically flat.

Fortunately, problems of this kind have been studied – see, e.g., [47]. To take the non-linear corrections into account, the procedure is as follows. Let us express $\delta N, \delta Y, \delta U$ in terms of three functions Z_0, Z_+, Z_- :

$$\begin{aligned}\delta N &= Z_0 + \kappa_1 \frac{1+r}{r} Z_+ + \kappa_1 \frac{1-r}{r} Z_-, \\ \delta Y &= Z_0 - \kappa_2 \frac{1+r}{r} Z_+ - \kappa_2 \frac{1-r}{r} Z_-, \\ \delta U &= \frac{1+r+r^2}{r^2} Z_+ + \frac{1-r+r^2}{r^2} Z_-.\end{aligned}\tag{7.5}$$

Eqs.(7.2) then assume the form

$$\begin{aligned}Z'_0 + \frac{Z_0}{r} &= \mathcal{S}_0(r, Z_0, Z_\pm) \equiv \kappa_1 \mathcal{N}_Y + \kappa_2 \mathcal{N}_N, \\ Z'_+ + Z_+ &= \mathcal{S}_+(r, Z_0, Z_\pm) \equiv \frac{r^2 - r + 1}{2r^2} (\mathcal{N}_N - \mathcal{N}_Y) + \frac{r-1}{2r} \mathcal{N}_U, \\ Z'_- - Z_- &= \mathcal{S}_-(r, Z_0, Z_\pm) \equiv \frac{r^2 + r + 1}{2r^2} (\mathcal{N}_Y - \mathcal{N}_N) + \frac{r+1}{2r} \mathcal{N}_U.\end{aligned}\tag{7.6}$$

Terms on the left in these equations are linear in Z_0, Z_\pm , while those on the right are non-linear. Neglecting the non-linear terms, the solution is $Z_0 = 1/r$, $Z_+ = e^{-r}$, $Z_- = e^{+r}$, and if we set

$$Z_0 = \frac{A}{r}, \quad Z_+ = B e^{-r}, \quad Z_- = 0,\tag{7.7}$$

this reproduces the linear part of (7.4). Now, to take the non-linear terms into account, one

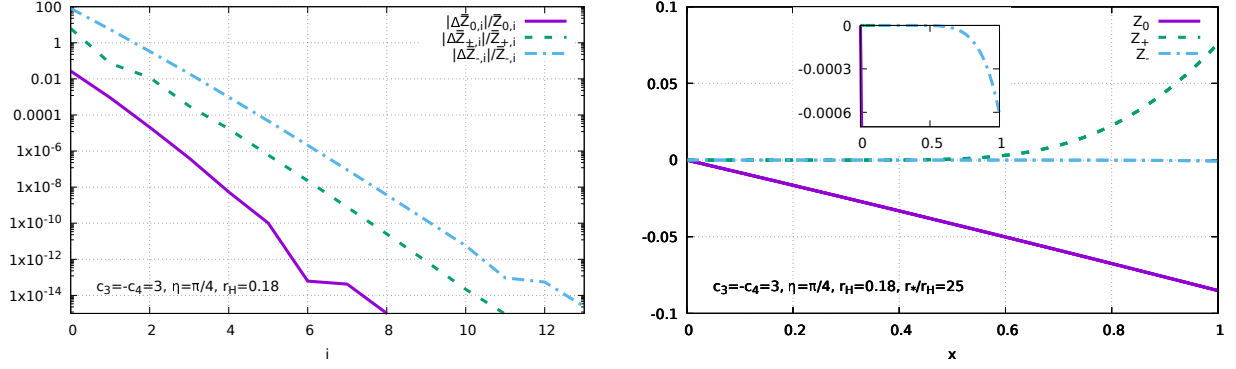


FIG. 1. Left panel: convergence of the iterations of the integral equations (7.8). Right panel: the amplitudes Z_0 , Z_{\pm} against $x = r_*/r$, where the insertion shows zoomed Z_- .

converts Eqs.(7.6) into the equivalent set of integral equations,

$$\begin{aligned}
 Z_0(r) &= \frac{A}{r} - \int_r^\infty \frac{\bar{r}}{r} \mathcal{S}_0(\bar{r}, Z_0(\bar{r}), Z_{\pm}(\bar{r})) d\bar{r}, \\
 Z_+(r) &= B e^{-r} + \int_{r_*}^r e^{\bar{r}-r} \mathcal{S}_+(\bar{r}, Z_0(\bar{r}), Z_{\pm}(\bar{r})) d\bar{r}, \\
 Z_-(r) &= - \int_r^\infty e^{r-\bar{r}} \mathcal{S}_-(\bar{r}, Z_0(\bar{r}), Z_{\pm}(\bar{r})) d\bar{r},
 \end{aligned} \tag{7.8}$$

where r_* is some large value. These equations determine the solution for $r > r_*$, and they are solved by iterations. To start the iterations, one neglects the non-linear terms, which gives the configuration (7.7). The next step is to inject this configuration to the integrals, which gives the corrected configuration, and so on. In practice, one introduces variables $x = r_*/r$ and $\bar{x} = r_*/\bar{r}$ assuming values in the interval $[0, 1]$, and then one discretizes the interval to compute the integrals.

To see the convergence of the iterations, we compute for each Z and for each discretization point the difference $\Delta Z_i = Z_{i+1} - Z_i$ of the results of the consecutive $(i+1)$ -th and i -th iterations, and then we take the average $\overline{\Delta Z_i}$ over all discretization points. Computing similarly the average \bar{Z}_i of Z_i , the ratios $\overline{\Delta Z_i}/\bar{Z}_i$ decrease with i exponentially fast, as seen on the left panel in Fig.1, hence the iterations converge. The solution of the integral equations is shown on the right panel in Fig.1: the amplitudes Z_0 and Z_{\pm} against $x = r_*/r$ (for $r_* = 25 r_H$). One can see that the amplitude Z_- is always small but non-vanishing, and that all the three amplitudes vanish for $x = 0$, hence the solution is indeed asymptotically flat.

This yields an asymptotically flat solution in the region $r > r_*$. To extend this solution to

the region $r_H < r < r_*$ one only needs its values at $r = r_*$,

$$\begin{aligned} Z_0(r_*) &= \frac{A}{r_*} - \int_{r_*}^{\infty} \frac{\bar{r}}{r} \mathcal{S}_0(\bar{r}, Z_0(\bar{r}), Z_{\pm}(\bar{r})) d\bar{r}, & Z_+(r_*) &= B e^{-r_*}, \\ Z_-(r_*) &= - \int_{r_*}^{\infty} e^{r_* - \bar{r}} \mathcal{S}_-(\bar{r}, Z_0, Z_{\pm}) d\bar{r}. \end{aligned} \quad (7.9)$$

To recapitulate, the described above procedure yields the boundary values for the fields at a large r_* and makes sure that the solution for $r > r_*$ exists and is indeed asymptotically flat. It is worth noting that the parameter A determines the ADM mass,

$$M = -A. \quad (7.10)$$

VIII. Numerical procedure

Summarizing the above discussion, the asymptotically flat black holes are described by solutions of the three coupled first order ODE's (4.23) for the three functions $N(r), Y(r), U(r)$ (which determines also $Q(r), q(r)$) with the following boundary conditions. At the horizon $r = r_H$ one has

$$N(r) = \sqrt{1 - \frac{r_H}{r}} \nu(r), \quad Y(r) = \sqrt{1 - \frac{r_H}{r}} y(r), \quad (8.1)$$

where the horizon values $\nu(r_H) \equiv \nu_H$ and $y(r_H) \equiv y_H$ are finite and determined by the Eqs. (A.8), (A.6) in Appendix A, while $U(r_H) \equiv U_H \equiv u_{r_H}$ can be arbitrary. Therefore, all possible boundary conditions at the horizon are labeled by just one free parameter u , and choosing some value for it, the equations can be integrated directly from the horizon, as explained in Appendix A, to the outer region $r > r_H$.

Far from the horizon, at $r = r_* \gg r_H$, one has

$$\begin{aligned} N(r_*) &= 1 + Z_0(r_*) + \kappa_1 B \frac{1 + r_*}{r_*} e^{-r_*} + \kappa_1 \frac{1 - r_*}{r_*} Z_-(r_*), \\ Y(r_*) &= 1 + Z_0(r_*) - \kappa_2 B \frac{1 + r_*}{r_*} e^{-r_*} - \kappa_2 \frac{1 - r_*}{r_*} Z_-(r_*), \\ U(r_*) &= r_* + B \frac{1 + r_* + r_*^2}{r_*^2} e^{-r_*} + \frac{1 - r_* + r_*^2}{r_*^2} Z_-(r_*), \end{aligned} \quad (8.2)$$

where $Z_0(r_*)$ and $Z_-(r_*)$ are functions of A, B determined by (7.9) via iterating the integral equations (7.8).

As a result, we have the boundary conditions at $r = r_H$ labeled by u and the boundary conditions at $r = r_*$ labeled by A, B . We use them to construct solutions in the region $r_H \leq r \leq r_*$. To this end, we choose some value of u and integrate numerically the equations starting from $r = r_H$ as far as some $r = r_0 < r_*$ and we obtain at this point some values which

will depend on r_H and u :

$$N(r_0) \equiv N_{\text{hor}}(r_H, u), \quad Y(r_0) \equiv Y_{\text{hor}}(r_H, u), \quad U(r_0) \equiv U_{\text{hor}}(r_H, u). \quad (8.3)$$

Then we choose A and B and numerically extend the large r data (8.2) from $r = r_*$ down to $r = r_0$, thereby obtaining

$$N(r_0) \equiv N_{\text{inf}}(A, B), \quad Y(r_0) \equiv Y_{\text{inf}}(A, B), \quad U(r_0) \equiv U_{\text{inf}}(A, B). \quad (8.4)$$

If the two sets of values agree, hence if

$$\begin{aligned} \Delta N(r_H, u, A, B) &\equiv N_{\text{hor}}(r_H, u) - N_{\text{inf}}(A, B) = 0, \\ \Delta Y(r_H, u, A, B) &\equiv Y_{\text{hor}}(r_H, u) - Y_{\text{inf}}(A, B) = 0, \\ \Delta U(r_H, u, A, B) &\equiv U_{\text{hor}}(r_H, u) - U_{\text{inf}}(A, B) = 0, \end{aligned} \quad (8.5)$$

then the solution in the interval $r \in [r_H, r_0]$ merges smoothly with the solution in the interval $r \in [r_0, r_*]$ to represent one single solution in the interval $r \in [r_H, r_*]$. The extension to the region $r > r_*$ is then provided by the integral equations (7.8), finally yielding an asymptotically flat black hole solution in the region $r \in [r_H, \infty)$. It is worth noting that these solution will depend neither on r_0 nor on r_* ; these values could be varied without affecting the global solution (which is a good consistency check).

In some cases using just two zones $[r_H, r_0]$ and $[r_0, r_*]$ produces too large numerical errors. To keep the numerical instability under control, one should then integrate through many smaller zones $[r_H, r_0], [r_0, r_1], [r_1, r_2] \dots [r_k, r_*]$ and perform matchings at $r_0, r_1, \dots r_k$ (see Sec.7.3.5 in [53]). This yields numerically stable results.

In the case of just two zones, the problem reduces to solving the matching conditions (8.5) by adjusting the values u, A, B . At least one solution to these three conditions certainly exists and corresponds to the Schwarzschild solution, for which

$$u = 1, \quad A = -\frac{r_H}{2}, \quad B = 0. \quad (8.6)$$

Are there other solutions ? Since there are three matching conditions for the three variables, their solutions must constitute a *discrete* set of points (u_k, A_k, B_k) in the 3-space spanned by u, A, B . This implies that different black hole solutions with the same r_H are *parametrically isolated* from each other. This creates a problem, since in order to solve numerically algebraic equations (8.5), an input configuration u, A, B is needed to start the numerical iterations within the Newton-Raphson procedure [39]. However, unless the input configuration is close to the solution, the numerical iterations do not converge, hence some additional information is necessary to specify where to start the iterations.

As explained in the Introduction, the additional information is provided by the stability analysis of the Schwarzschild solution (1.2) [33, 42]. In this analysis one considers the two metrics of the form (4.2) with

$$\begin{aligned} Q &= S + \delta Q, & N &= S + \delta N, & R &= r \\ q &= S + \delta q, & Y &= S + \delta Y, & U &= r + \delta U, & f_{01} &= \delta\alpha, \end{aligned} \quad (8.7)$$

where $S = \sqrt{1 - \frac{r_H}{r}}$ while the perturbations $\delta Q, \delta N, \delta q, \delta Y, \delta U, \delta\alpha$ are assumed to be small and depend on t, r . It turns out that at the GL point, for $r_H = 0.86$, the perturbation equations admit a *static* solution (zero mode) for which $\delta Q, \delta N, \delta q, \delta Y, \delta U$ depend only on r and are bounded everywhere in the region $r \geq r_H$ while $\delta\alpha = 0$. This solution can be viewed as a perturbative approximation of a new solution that merges with the Schwarzschild solution for $r_H = 0.86$.

This suggests that to get new solutions of the matching conditions (8.5), one should choose the event horizon size to be close $r_H = 0.86$ and choose the input configuration u, A, B to be close to (8.6). Then the numerical iterations should converge to values u, A, B which are slightly different from (8.6) and correspond to an almost Schwarzschild black hole slightly distorted by a massive hair. Changing then iteratively the value of r_H yields solutions which deviate considerably from the Schwarzschild metric close to the horizon, but always approach flat metric in the asymptotic region.

IX. Asymptotically flat hairy black holes

Applying the procedure outlined above, we were able to construct asymptotically flat hairy solutions. We confirm the results of Ref. [44] and obtain many new results.

First of all, we find that for r_H approaching from below the GL value, $r_H \approx 0.86$, there are asymptotically flat hairy black hole solutions for any c_3, c_4, η . They are very close to the Schwarzschild solution: one has $u = U_H/r_H \approx 1$ and the ADM mass $M \approx r_H/2$. However, for smaller values of r_H the solutions deviate more and more from Schwarzschild. To illustrate this, we plot in Fig. 2 the functions $N/S, Q/S, Y/S, q/S$, and U' . If these functions all equal to one, then the solution is Schwarzschild. As one can see, they indeed approach unity far away from the horizon, but close to the horizon they deviate considerably from unity, hence the massive graviton hair is concentrated in this region.

Solutions are regular for r_H close to 0.86, however, for smaller r_H and depending on values of c_3, c_4, η , the amplitudes Y, q, U' may show additional zeros outside the horizon, whereas Q, N always remain positive. This implies that the f-metric is singular, because the invariants

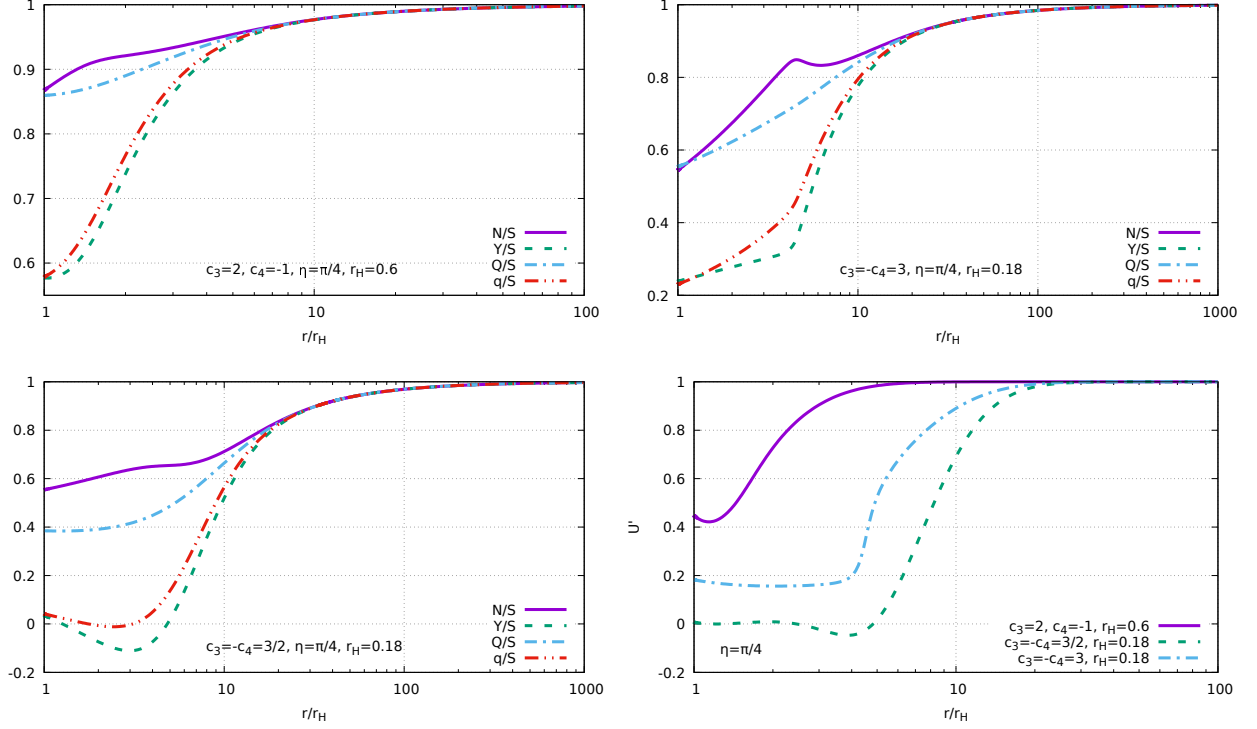


FIG. 2. Profiles of N/S , Y/S , Q/S , q/S with $S = \sqrt{1 - r_H/r}$ and that of U' for solutions with $\eta = \pi/4$ but for various values of r_H, c_3, c_4 . Solution with $c_3 = -c_4 = 3/2$ shown on the two lower panels is singular because the amplitudes q, Y, U' develop zeros outside the horizon.

of its Riemann tensor diverge where the zeros are located. An example of this is shown on the lower two panels in Fig. 2. As seen in Fig. 3 where results for different values of η are shown, small r_H solutions become singular when η approaches $\pi/2$, but they are regular for small η .

Solutions in Fig. 2 are shown up to large but still finite values of the radial coordinate, $r/r_H \leq 100$ or $r/r_H \leq 1000$. What is shown is the combination of the solutions of differential equations (4.23) in the region $r_H \leq r \leq r_*$ and of the integral equations (7.6) for $r > r_*$ where $r_*/r_H = 25$. At the same time, our procedure yields solutions in the whole region $r \in [r_H, \infty)$. Introducing the compactified radial variable

$$\xi = \frac{r - r_H}{r + r_H} \in [0, 1], \quad (9.8)$$

we plot in Fig. 3 the amplitudes N, Y, Q, q against ξ . As seen, the amplitudes approach unity as $\xi \rightarrow 1$ (same is true for U') hence the solutions are indeed asymptotically flat. The disadvantage of this parameterization is that the slope of the functions does not vanish for $\xi \rightarrow 1$. Indeed, for large r one has $N = 1 - M/r + \dots$ and $\xi = 1 - r_H/r + \dots$ hence at infinity $dN/d\xi = M/r_H$.

If $\eta = \pi/2$ then $\kappa_1 = 0$ and the g-metric becomes Schwarzschild. The theory reduces then to the massive gravity for the dynamical f-metric on a fixed Schwarzschild background. The

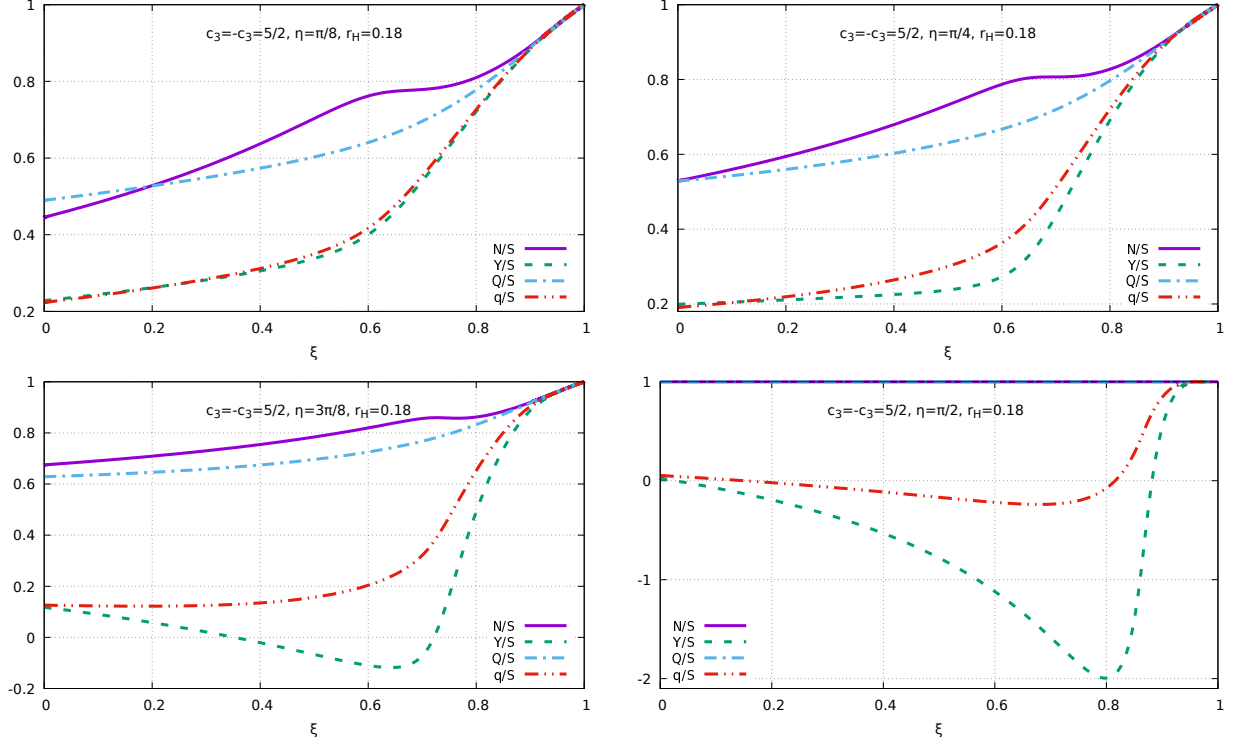


FIG. 3. Profiles of N/S , Y/S , Q/S , q/S with $S = \sqrt{1 - r_H/r}$ against $\xi = (r - r_H)/(r + r_H)$ for solutions with the same c_3, c_4, r_H but for different values of η . Solutions are regular for small η , but for larger η the amplitude Y shows zeros, hence the f-metric is singular. For $\eta = \pi/2$ the g-metric is Schwarzschild with $N/S = Q/S = 1$.

solution for the f-metric is shown on the lower right panel in Fig. 3. Similarly, for $\eta = 0$ one has $\kappa_2 = 0$ and the f-metric is Schwarzschild, while the g-metric is a solution of the massive gravity on the Schwarzschild background shown on the upper left panel in Fig. 4. One should emphasise that the radii of the background Schwarzschild black holes for $\eta = 0$ and for $\eta = \pi/2$ are not the same. For example, for $\eta = \pi/2$ the Schwarzschild black hole has $r_H = 0.18$ for the solution shown in Fig. 3, while for $\eta = 0$ the event horizon size is determined not by r_H but by $U_H = ur_H$ where $u \approx 7$ (as seen in Fig. 4) hence this time the Schwarzschild black hole is much larger. As a result, solutions on these different backgrounds look quite different – the solution for the f-metric on the lower right panel in Fig. 3 shows zeros hence is singular, while the solution for the g-metric on the upper left panel in Fig. 4 is regular.

Fig. 4 shows the η -dependence of $u = U_H/r_H$, of the ADM mass M expressed in units of the Schwarzschild mass $M_S = r_H/2$, and of the temperature T expressed in units of the Schwarzschild temperature $T_S = 1/(4\pi r_H)$. As one can see, the dependence is rather strong for small r_H , in particular for u . The decrease of the mass M with η can be understood by noting that the mass is the same with respect to each metric (the same is true for the

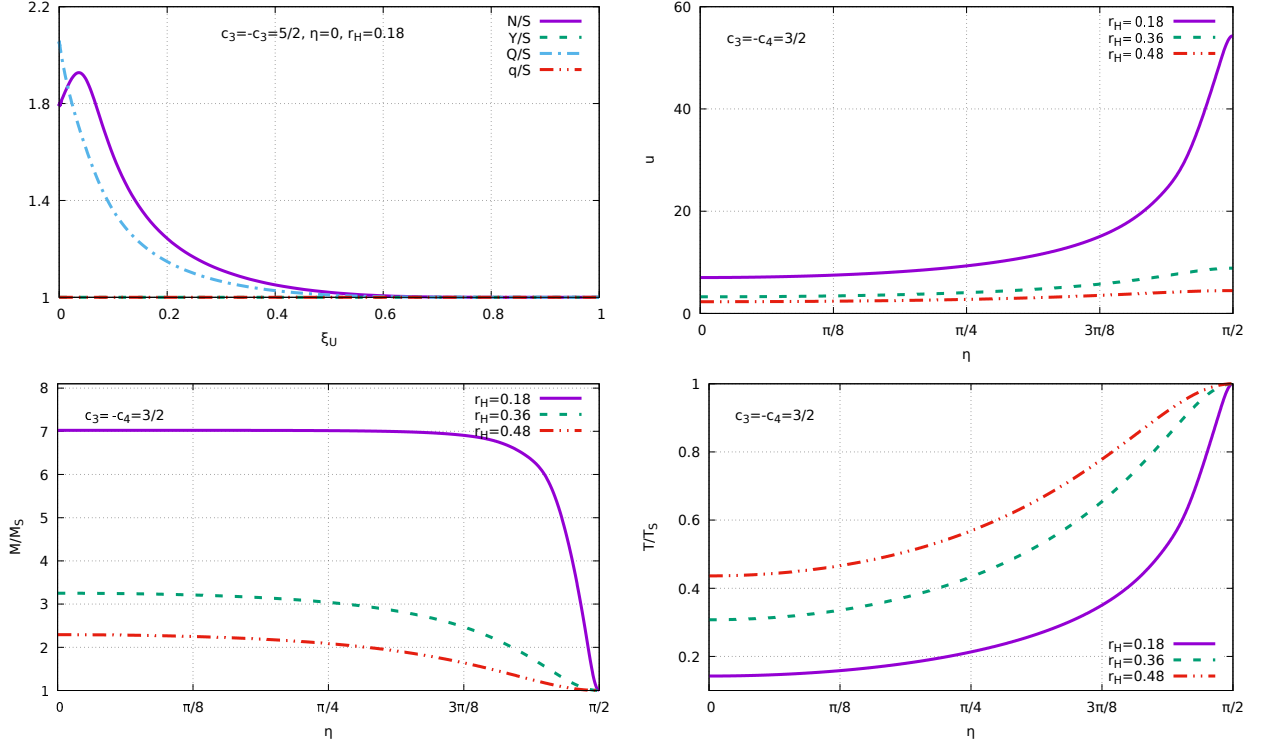


FIG. 4. Upper left panel: N/S , Y/S , Q/S , q/S with $S = \sqrt{1 - U_H/U}$ against the compact variable $\xi_U = (U - U_H)/(U + U_H)$ for $\eta = 0$. One has $Y/S = q/S = 1$ hence the f-metric is Schwarzschild. The other three panels show $u = U_H/r_H$, the ADM mass M , and the temperature T against η .

temperature). If $\eta = \pi/2$ then the g-metric is Schwarzschild hence $M = M_S$ and $T = T_S$. If $\eta = 0$ then the f-metric is Schwarzschild with a larger radius $U_H = ur_H$, hence the mass is larger, $M = U_H/2 = uM_S$, while the temperature is smaller, $T = T_S/u$. Therefore, if $\eta = 0$ then $M/M_S = u$ so that, for example, $u \approx 7$ for $r_H = 0.18$, as seen in Fig. 4.

Fig. 5 shows the dependence of u and M on $c_3 = -c_4$. As one can see, the solutions exist if only the value of $c_3 = -c_4$ is not too small. Similarly, not all hairy black holes exist for however small values of r_H . As was noticed in [44], small r_H black holes exist if the coefficient b_3 in the potential (2.4) vanishes so that the cubic part of the potential is absent. In view of (2.15), this requires that $c_3 = -c_4$, but this is not the only condition. Depending on the parameter values, one can distinguish the following two cases:

$$\text{I : } c_3 \neq -c_4 \text{ or } c_3 = -c_4 < 2, \quad \text{II : } c_3 = -c_4 \geq 2. \quad (9.9)$$

In case I asymptotically flat hairy black hole exist only for $0 < r_H^{\min} < r_H < 0.86$ hence they cannot be arbitrarily small. In case II they exist for any $0 < r_H < 0.86$, although their f-metric may be singular for small r_H . We shall explain below in Section XI what happens when r_H approaches the lower bound.

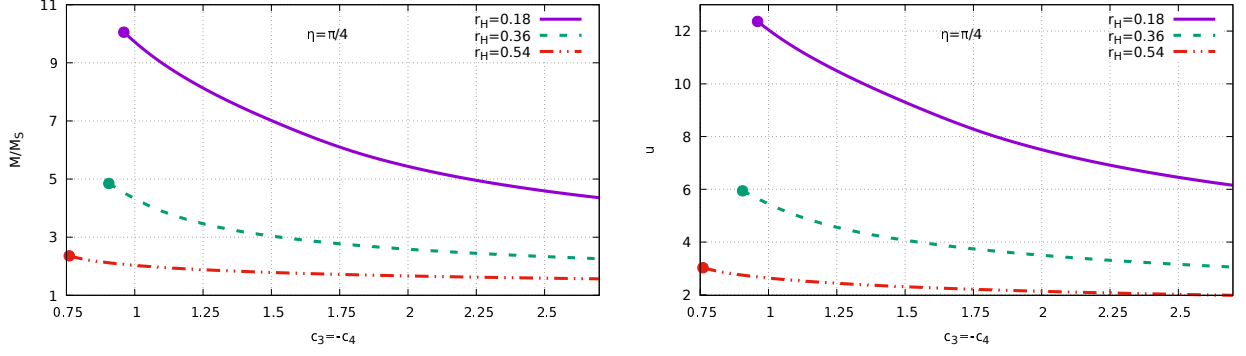


FIG. 5. The M/M_S (left) and $u = U_H/r_H$ (right) against $c_3 = -c_4$.

Duality relation

The results described above in this Section essentially reproduce those of Ref. [44], the only important difference is that we show solutions for different values of η , whereas Ref. [44] shows them only for $\eta = \pi/4$. However, starting from this moment and in the following two Sections we shall be describing new results.

Ref. [44] finds solutions only below the GL point, for $r_H \leq 0.86$. At the same time, the consistency of the procedure requires that there should be asymptotically flat hairy black holes also for $r_H > 0.86$. This follows from the symmetry (4.16) of the equations, which now reads

$$\eta \rightarrow \frac{\pi}{2} - \eta, \quad Q \leftrightarrow q, \quad N \leftrightarrow Y, \quad U \leftrightarrow r, \quad c_3 \rightarrow 3 - c_3, \quad c_4 \rightarrow 4c_3 + c_4 - 6. \quad (9.10)$$

More precisely, this means that if for some values of η, c_3, c_4 there is a solution

$$Q(r), q(r), N(r), Y(r), U(r), \quad (9.11)$$

then for $\tilde{\eta} = \pi/2 - \eta$, $\tilde{c}_3 = 3 - c_3$, $\tilde{c}_4 = 4c_3 + c_4 - 6$ there should be the “dual” solution described by

$$\tilde{Q}(r) = q(w(r)), \quad \tilde{q}(r) = Q(w(r)), \quad \tilde{N}(r) = Y(w(r)), \quad \tilde{Y}(r) = N(w(r)), \quad \tilde{U}(r) = w(r), \quad (9.12)$$

where $w(r)$ is the function inverse for $U(r)$ such that $U(w(r)) = r$. This duality correspondence relates to each other black holes of difference size, since (4.24) has the horizon at $r = r_H$ while the horizon of (9.12) is located where $w(r) = r_H$ that is at $r = \tilde{r}_H = U(r_H)$. One has

$$\tilde{u} = \frac{\tilde{U}(\tilde{r}_H)}{\tilde{r}_H} = \frac{r_H}{U(r_H)} = \frac{1}{u}. \quad (9.13)$$

Now, for hairy solutions with $r_H < 0.86$ one always has $U(r_H) > 0.86$ and $u = U(r_H)/r_H > 1$. It follows that their duals are characterized by $\tilde{r}_H > 0.86$ and by $\tilde{u}_H < 1$.

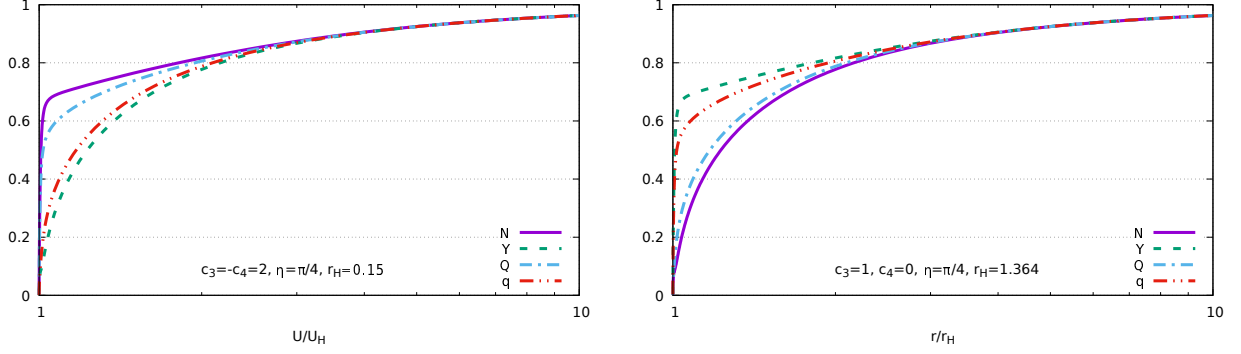


FIG. 6. The solution with $c_3 = -c_4 = 2$, $\eta = \pi/4$, $r_H = 0.15$ (left panel) and the dual solution with $c_3 = 1$, $c_4 = 0$, $\eta = \pi/4$, $r_H = 1.364$ (right panel). The curves on the two panels are exactly the same, up to the interchange $N \leftrightarrow Y$, $Q \leftrightarrow q$, $r/r_H \leftrightarrow U/U_H$.

An explicit example of the duality relation is shown in Fig. 6, which presents on the left panel the solution for $c_3 = -c_4 = 2$, $\eta = \pi/4$, $r_H = 0.15$ for which $U(r_H) = 1.364$, hence $u = 1.364/0.15 = 2.42$. The duality implies that for $c_3 = 1$, $c_4 = 0$, $\eta = \pi/4$ there must be the dual solution with $r_H = 1.364$ and $u = 0.15/1.364 = 0.41$, which is indeed confirmed by our numerics. Plotting the first solution against U/U_H and the second one against r/r_H , as shown in Fig. 6, yields exactly the same curves, up to the interchange $N \leftrightarrow Y$, $Q \leftrightarrow q$.

It is unclear why solutions with $r_H > 0.86$ were not found in [44].

The duality is in fact a powerful tool for studying the solutions, because sometimes their properties may look puzzling in one description but become completely obvious within the dual description.

X. Stability analysis

In this section we analyze the stability of the hairy solutions by studying their perturbations within the ansatz described in Appendix B,

$$\begin{aligned}
 ds_g^2 &= -Q^2 dt^2 + \frac{dr^2}{N^2} + r^2 d\Omega^2, \\
 ds_f^2 &= -(q^2 - \alpha^2 Q^2 N^2) dt^2 - 2\alpha \left(q + \frac{QNU'}{Y} \right) dt dr + \left(\frac{U'^2}{Y^2} - \alpha^2 \right) dr^2 + U^2 d\Omega^2, \quad (10.1)
 \end{aligned}$$

where Q , q , N , Y , α , U are functions of r and t . The full set of the field equations in this case is shown in Appendix B. If we set $\alpha = 0$ and assume that nothing depends on time, then we return back to the static case studied above. Therefore, small deviations from the static

solutions are described by (10.1) with

$$\begin{aligned}
Q(r, t) &= Q^{(0)}(r) + \delta Q(r, t), \\
q(r, t) &= q^{(0)}(r) + \delta q(r, t), \\
N(r, t) &= N^{(0)}(r) + \delta N(r, t), \\
Y(r, t) &= Y^{(0)}(r) + \delta Y(r, t), \\
U(r, t) &= U^{(0)}(r) + \delta U(r, t), \\
\alpha(r, t) &= \delta \alpha(r, t),
\end{aligned} \tag{10.2}$$

where the functions $Q^{(0)}(r)$, $q^{(0)}(r)$, $N^{(0)}(r)$, $Y^{(0)}(r)$, $U^{(0)}(r)$ correspond to the background black hole solution while the perturbations $\delta Q, \delta q, \delta N, \delta Y, \delta U, \delta \alpha$ are small.

We therefore inject (10.2) to Eqs.(B.5), (B.6) and linearize with respect to the perturbations. Linearizing the $G_1^0(g) = \kappa_1 T_1^0$ equation then yields

$$\frac{2}{rNQ^2} \delta \dot{N} = \kappa_1 \frac{\mathcal{P}_1}{Q} \delta \alpha, \tag{10.3}$$

where N, Q, \mathcal{P}_1 relate to the static background, and we do not write their over-sign “(0)” for simplicity. Since all linear perturbations are assumed to have the harmonic time-dependence,

$$\delta N(t, r) = e^{i\omega t} \delta N(r) \quad \delta \alpha(t, r) = e^{i\omega t} \delta \alpha(r), \tag{10.4}$$

one obtains the algebraic relation

$$\delta \alpha(r) = \frac{2i\omega}{rNQ\mathcal{P}_1} \delta N(r). \tag{10.5}$$

Linearizing similarly the $G_1^0(f) = \kappa_2 \mathcal{T}_1^0$ equation yields a linear relation between $\delta \alpha(r)$, $\delta Y(r)$, $\delta U(r)$. Using these two algebraic relations one finds that the three equations $G_0^0(g) = \kappa_1 T_0^0$, $G_0^0(f) = \kappa_2 \mathcal{T}_0^0$ and $\nabla_\mu^{(g)} T_0^\mu = 0$ yield upon the linearization three equivalent to each other relations. Therefore, among the 8 equations (B.5), (B.6) only 6 are independent (at least at the linearized level).

Taking all of this into account and linearizing similarly the remaining 3 equations $G_1^1(g) = \kappa_1 T_1^1$, $G_1^1(f) = \kappa_2 \mathcal{T}_1^1$ and $\nabla_\mu^{(g)} T_1^\mu = 0$, one finds that all 6 perturbation amplitudes $\delta Q(r)$, $\delta q(r)$, $\delta N(r)$, $\delta Y(r)$, $\delta U(r)$ and $\delta \alpha(r)$ can be expressed in terms of a single master amplitude $\Psi(r)$ subject to the Schrödinger-type equation,

$$\frac{d^2 \Psi}{dr_*^2} + (\omega^2 - V(r)) \Psi = 0. \tag{10.6}$$

Here the potential $V(r)$ is a rather complicated function of the background amplitudes that we do not show explicitly, and the tortoise radial coordinate $r_* \in (-\infty, +\infty)$ is defined by the

relation

$$dr_* = \frac{1}{a(r)} dr, \quad (10.7)$$

where the function $a(r)$ (also complicated) varies from 0 to 1 as r changes from r_H to ∞ . The potential V always tends to zero at the horizon, for $r_* \rightarrow -\infty$, and it approaches unit value at infinity, for $r_* \rightarrow +\infty$. One should remember that our dimensionless variables are related to the dimensionfull ones via $r = mr$, $r_H = mr_H$, $V = m^2 V$, $\omega = \omega/m$.

In the Schwarzschild case, when the static background amplitudes are $Q = q = N = Y = \sqrt{1 - r_H/r}$ and $U = r$, one has $a(r) = Q^2(r)$ and the potential reduces to

$$V(r) = \left(1 - \frac{r_H}{r}\right) \left(1 + \frac{r_H}{r^3} + 6 \frac{r_H(r_H - 2r) + r^3(r - 2r_H)}{(r_H + r^3)^2}\right), \quad (10.8)$$

in agreement with Ref. [42]. In the flat space limit $r_H \rightarrow 0$ this reduces to $V(r) = 1 + 6/r^2$, which is the potential of a massive particle of unit mass (in units of the graviton mass) with spin $s = 2$.

Eq.(10.6) defines the eigenvalue problem on the line $r_* \in (-\infty, +\infty)$. Solutions of this problem with $\omega^2 > 0$ describe scattering states of gravitons. In addition, there can be bound states with purely imaginary frequency $\omega = i\sigma$ and hence with $\omega^2 = -\sigma^2 < 0$. For such solutions the wavefunction Ψ is everywhere bounded and square-integrable, because one has $e^{+\sigma r_*} \leftarrow \Psi \rightarrow e^{-\sqrt{1+\sigma^2} r_*}$ as $-\infty \leftarrow r_* \rightarrow +\infty$, respectively. Such bound state solutions grow in time as $e^{i\omega t} = e^{\pm\sigma t}$. Therefore, they correspond to unstable modes of the background black holes.

Computing the eigenfrequencies

Our aim is to investigate a potential existence of negative modes with $\omega^2 < 0$ in the spectrum of the eigenvalue problem (10.6). If such modes exist, then the background black holes are unstable. If they do not exist, then the black holes are stable with respect to spherically symmetric perturbations, which strongly suggests that they should be stable with respect to all perturbations. Indeed, in most known cases the S -channel is usually the only place where the instability can reside (of course, this should be proven case to case).

The first thing to check is the shape of the potential $V(r)$, because if it is everywhere positive, then there are no bound states. We therefore show in Fig.7 the potential $V(r)$ for the hairy backgrounds for several values of the event horizon size r_H and for different c_3, c_4 , and we also show $V(r)$ for the Schwarzschild solution with the same r_H (it does not depend on c_3, c_4). We observe that in each case the potential vanishes at the horizon, then shows negative

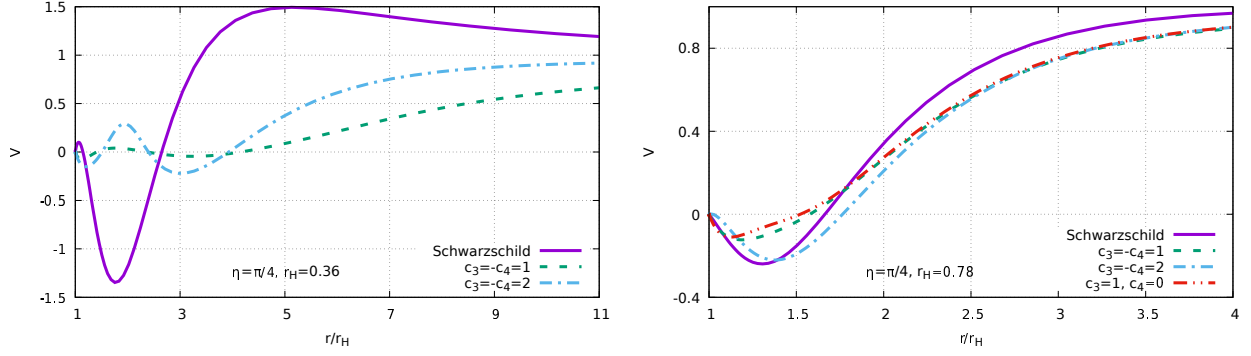


FIG. 7. Potential $V(r)$ for $r_H = 0.36$ (left) and $r_H = 0.78$ (right) for different c_3, c_4 with $\eta = \pi/4$.

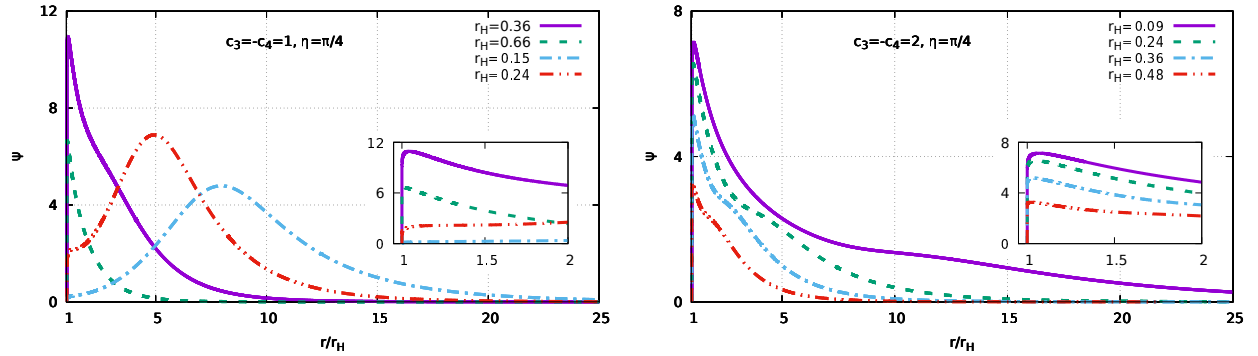


FIG. 8. Negative mode eigenfunctions $\Psi(r)$ for $\eta = \pi/4$ and different r_H , with $c_3 = -c_4 = 1$ (left panel) and $c_3 = -c_4 = 2$ (right panel). They vanish at the horizon and at infinity.

values in its vicinity, and then approaches unity as $r \rightarrow \infty$. Therefore, since the potential is not positive definite, bound states *may* exist, but their existence is not yet guaranteed.

We know that a bound state certainly exists for the Schwarzschild background with $r_H < 0.86$ [33, 42]. When looking at the potentials for the hairy solution with $r_H = 0.78$ in Fig. 7, we notice that they are close to the Schwarzschild potential, hence a bound state could exist for these potentials as well.

In order to know whether bound states exist or not, one can use the well-known Jacobi criterion [54] and construct the solution of the Schrödinger equation (10.6) with $\omega = 0$. If this solution $\Psi(r)$ crosses zero somewhere, then there are bound states. We start in the asymptotic region where the tortoise coordinate r_* becomes identical to the usual r , hence Eq.(10.6) reduces simply to $\Psi'' = \Psi$ so that the bounded solution is $\Psi = e^{-r}$. Then we extend this solution numerically toward small values of r , and we find that, depending on values of r_H, η, c_3, c_4 , it may indeed show a zero as r approaches r_H . Therefore, there exists a bound state.

The next step is to actually find the bound state by solving the eigenvalue problem (10.6)

with the potential $V(r)$ obtained by numerically solving the background equations. For this we set $\omega^2 = -\sigma^2$ and determine the local solutions at infinity and close to the horizon,

$$B(r - r_H)^{\sigma r_H} \leftarrow \Psi(r) \rightarrow e^{-\sqrt{1+\sigma^2}r} \quad \text{as} \quad r_H \leftarrow r \rightarrow \infty, \quad (10.9)$$

where B is an integration constant. Then we apply the multiple shooting method and numerically extend the solution on the left toward large r , extending at the same time the solution on the right toward small r . The two solutions meet at some intermediate point $r = r_0$, where the values of $\Psi(r_0)$ and $\Psi'(r_0)$ should agree. This gives two conditions which are fulfilled by adjusting the values two parameters B and σ in (10.9), which finally yields the bound state solution (see [55, 56] for a review on BHs perturbation theory and the tools that can be used to solve the perturbation equation).

The eigenfunctions Ψ against the ordinary radial coordinate r are shown in Fig.8. They vanish at the horizon then show a maximum, sometimes very close to the horizon, and then zero again for $r \rightarrow \infty$.

As a result, we find the eigenfrequencies $\omega^2 < 0$ and the corresponding eigenfunctions $\Psi(r)$ for all hairy black holes obtained in [42]. Therefore, all these solutions are unstable. It is worth emphasising that all of them correspond to the particular choice $\eta = \pi/4$, hence $\kappa_1 = \kappa_2 = 1/2$. In order to test our method, we have also computed the negative mode for the Schwarzschild solution [42].

As seen in Fig.9, the absolute value of the negative mode eigenvalue for the Schwarzschild solution is always larger than that for the hairy solutions. Therefore, the instability growth rate for the hairy black holes is not as large as for the Schwarzschild solution. In all cases, since one has $\omega = \boldsymbol{\omega}/m$ where $\boldsymbol{\omega}$ is the dimensionful physical frequency, the instability growth time is $1/\boldsymbol{\omega} = 1/(\boldsymbol{\omega}m)$. If we assume the graviton mass m to be very small and given by (5.5), then the instability growth time will be cosmologically large, hence the instability will not play any role. However, as we shall see below, it is preferable to assume that $1/m \sim 10^6$ km according to (5.7), in which case the instability growth time will be of the order of 10^3 seconds, hence the instability is dangerous and should be avoided.

As seen in Fig.9, the eigenvalue $\omega^2(r_H) < 0$ approaches zero when $r_H \rightarrow 0.86$, therefore all hairy black holes become then stable. However, they are no longer hairy in this limit – they “lose their hair” and merge with the Schwarzschild solution. Near $r_H = 0.86$ all solutions are close to each other and ω^2 is close to zero for any c_3, c_4, η , while for smaller r_H the backgrounds and ω^2 become parameter-dependent. The eigenvalue $\omega^2(r_H) < 0$ may approach zero also for type I solutions for a small $r_H \neq 0$ when they cease to exist. For example, for $c_3 = 1, c_4 = 0$, the hairy solution disappear at $r_H \sim 0.58$, and at the same time the eigenvalue ω^2 approaches

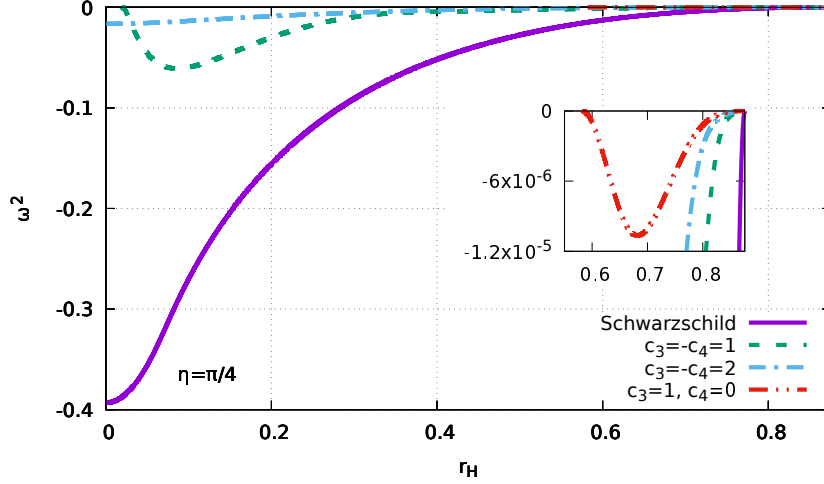


FIG. 9. The negative mode eigenvalue $\omega^2(r_H)$ for the hairy and Schwarzschild black holes against r_H for different values of c_3, c_4 . In all cases $\eta = \pi/4$.

zero, as seen in the insertion in Fig.9.

The instability of hairy black holes is in fact somewhat puzzling, since it is unclear what they may decay into. Since the hairy solutions with $r_H < 0.86$ are more energetic than the Schwarzschild solution, they probably decay via absorbing and/or radiating away their hair and approaching the “bald” Schwarzschild solution. However, the latter is also unstable for $r_H < 0.86$ and should decay in its turn.

The perturbative instability of the Schwarzschild solution in the massive bigravity theory is mathematically equivalent [33] to the Gregory-Laflamme instability of the vacuum black string in D=5 [43]. It is known that the non-linear development of the latter leads to the formation of an infinite string of “black hole beads” in D=5, but the event horizon topology does not change [57]. This fact being established within the D=5 vacuum GR, a similar scenario is not possible in the D=4 bigravity theory, hence the fate of the bigravity black holes should be different. One possibility is that the black hole radiates away all of its energy within the S-channel (some radiative solutions are known explicitly [58, 59]), but it is unclear what happens to the horizon – if it disappears or not. In GR the horizon cannot disappear via a classical process [60], but in the bimetric theory the situation might be different.

Remarkably, we find that these puzzling issues are not omnipresent and the black holes can be stable for $\eta \neq \pi/4$. In Fig.10 we show ω^2 against η for several values of r_H for solutions with $c_3 = -c_4 = 2$. One can see that $\omega^2(\eta) < 0$ approaches zero and the negative mode disappears when η approaches $\pi/2$. The background solutions then do not disappear and become stable. However, the f-metric becomes then singular and shows oscillations of the amplitudes Y, q, U' ,

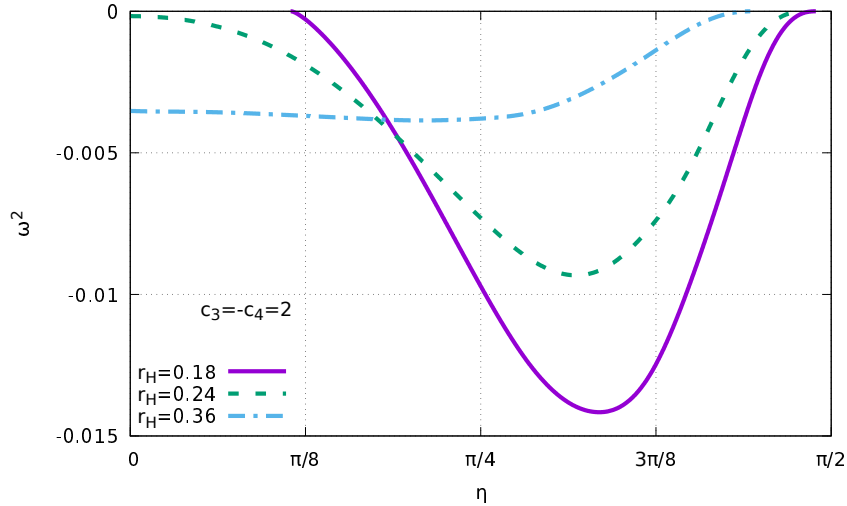


FIG. 10. The negative mode eigenvalue $\omega^2(\eta)$ for the hairy black holes with $c_3 = -c_4 = 2$.

as seen in Fig.3, hence this case is not interesting. At the same time, ω^2 approaches zero also when η become small enough, if only r_H is also small, as seen in Fig.10. The background solutions then become stable and remain regular.

Summarizing the above discussion, for some parameter values the hairy black holes are unstable, but for other parameter values they can be stable and regular. Below we shall describe a parameter choice leading to a large set of stable and regular solutions.

XI. Parameter values and the physical solutions

In this Section we give a detailed description of particular subsets of solutions. Providing a complete classification of solutions depending on 4 parameters r_H, η, c_3, c_4 would be a very difficult task. We therefore adopt the following strategy: choosing the particular values

$$c_3 = -c_4 = -5/2 \quad (11.1)$$

which fulfil condition II in (9.9), we study the solutions for all possible r_H, η . Performing next the duality transformation gives us all possible solutions for values

$$c_3 = 1/2, \quad c_4 = 3/2, \quad (11.2)$$

which fulfil condition I in (9.9). This approach reveals interesting and rather complex features which are presumably generic for solutions with any c_3, c_4 .

Fig. 11 shows the ADM mass $M(r_H)$ and the function $U_H(r_H)$ for several values of $\eta \in [0, \pi/2]$. As one can see, all curves $M(r_H)$ intersect at the GL point, $(r_H, M_H) = (0.86, 0.43)$,

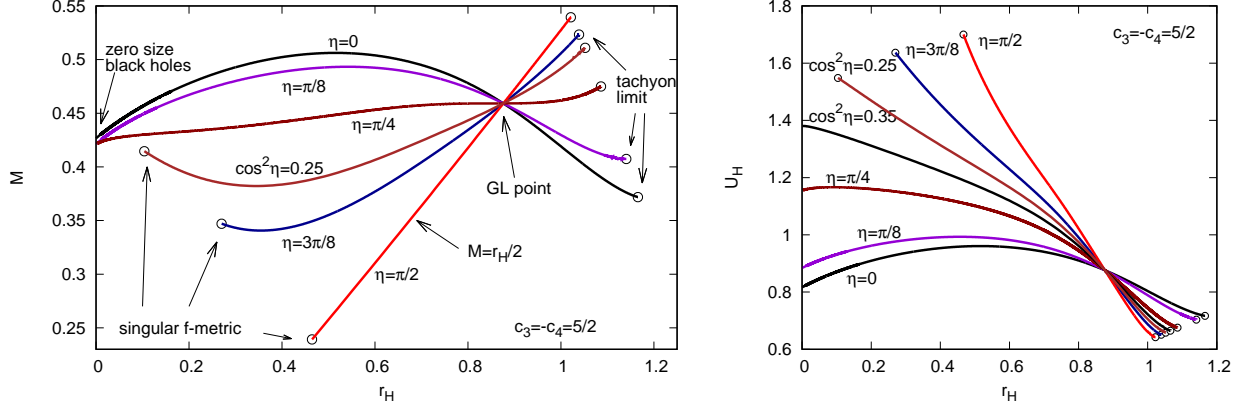


FIG. 11. The mass $M(r_H)$ (left) and the functions $U_H(r_H)$ (right) for the hairy black hole solutions with $c_3 = -c_4 = -5/2$

where all solutions bifurcate with the Schwarzschild solution

$$N^2 = Q^2 = Y^2 = q^2 = 1 - \frac{0.86}{r}, \quad U = r, \quad (11.3)$$

whereas all curves $U_H(r_H)$ pass through the point $(r_H, U_H) = (0.86, 1)$. Away from the bifurcation point, the g-metric still remains Schwarzschild if $\eta = \pi/2$, in which case $M(r_H)$ is a linear function,

$$\eta = \frac{\pi}{2} : \quad N^2 = Q^2 = 1 - \frac{r_H}{r} \quad \Rightarrow \quad M = \frac{r_H}{2}, \quad (11.4)$$

but the f-metric for these solutions is not Schwarzschild, even though both metrics have the same mass. (The f-metric for $\eta = \pi/2$ shown in Fig. 3 (right-lower panel) is singular since q, Y oscillate, but the digram in Fig. 11 takes into account only values of r_H corresponding to regular solutions.) For $\eta \neq \pi/2$ the mass depends non-linearly on r_H .

Introducing the mass function $M(r)$ via $N^2(r) = 1 - 2M(r)/r$, the $G^0_0(g) = \kappa_1 T^0_0$ Einstein equation in (2.18) assumes the form

$$M'(r) = \frac{\kappa_1}{2} r^2 T^0_0, \quad (11.5)$$

from where the ADM mass

$$M = M(\infty) = \frac{r_H}{2} + \frac{\kappa_1}{2} \int_{r_H}^{\infty} T^0_0 r^2 dr \equiv M_{\text{bare}} + M_{\text{hair}}. \quad (11.6)$$

Here the “bare” mass $M_{\text{bare}} = r_H/2$ is determined only by the horizon radius and coincides with the mass of the $\eta = \pi/2$ solution, while the mass M_{hair} expressed by the integral is the contribution of the massive hair distributed outside the horizon. As one can see in Fig. 11, one has $M > r_H/2$ if $r_H < 0.86$, hence the “hair mass” is positive and the hairy solutions are more energetic than the bare Schwarzschild black hole. However, the mass of the hair becomes

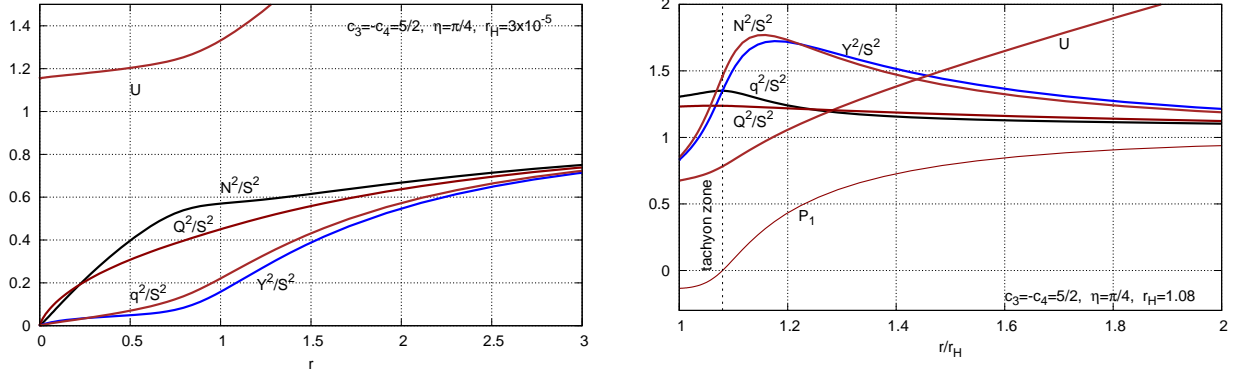


FIG. 12. Profiles of the solution with $r_H \sim 10^{-5}$ that is close to the zero size black hole (left), and of that close to the tachyon limit, with $D \sim 10^{-6}$ (right). One has $S^2 = 1 - r_H/r$.

negative above the GL point, where $r_H > 0.86$, and the hairy solutions are then less energetic than the bare one. Therefore the energy density T_0^0 can be negative. In fact, there are no reasons for which the standard energy conditions should be respected within the bigravity theory.

Each curve in Fig. 11 is defined only in a finite interval $r_H \in [r_H^{\min}(\eta), r_H^{\max}(\eta)]$. The terminate points of the curves correspond to limits beyond which one cannot continue, and it is very instructive to understand what happens in these limits.

A. The singular lower limit $r_H \rightarrow r_H^{\min}(\eta)$

It turns out that $r_H^{\min}(\eta) > 0$ if $\eta > 0.93$ hence $\kappa_1 \leq 0.35$ (these values would be different for different c_3, c_4). In this case the f-metric of the limiting for $r_H \rightarrow r_H^{\min}(\eta)$ solutions becomes singular because the q, Y -amplitudes start to develop a second zero outside the horizon. This phenomenon has already been discussed above and is similar to what is shown in Figs. 2, 3. Solutions exist also for $r_H < r_H^{\min}(\eta)$ but they are all singular in the same sense and should be excluded. Therefore, one should require that $r_H > r_H^{\min}(\eta)$.

If $\eta < 0.93$ then $r_H^{\min}(\eta) = 0$ and the solutions extend down to arbitrarily small values of r_H . Remarkably, as seen in Fig. 11, the mass M does not vanish when $r_H \rightarrow 0$ but approaches a finite value, even though the bare mass $M_{\text{bare}} = r_H/2 \rightarrow 0$. Therefore, all mass is contained in the “hair mass” in this limit, hence something remains when the horizon size r_H shrinks to zero. A similar phenomenon is actually known, since in many non-linear field theories there are solutions describing a small black hole inside a soliton (for example, inside the magnetic monopole) [35]. Sending the horizon size to zero the black hole disappears, but its external non-linear matter fields remain and become the gravitating soliton containing in its center a

regular origin instead of the horizon. Therefore, the $r_H \rightarrow 0$ limit of such a hairy black hole is a regular soliton.

One may think that the situation could be similar also in our case, hence there should be a limiting configuration to which the black hole solutions approach pointwise when $r_H \rightarrow 0$. It seems that such a limiting solution indeed exists, however, it is singular and not of the regular soliton type. First, as seen in Fig. 11, the value of U_H which determines the size of the f-horizon remains finite when $r_H \rightarrow 0$, hence the f-geometry remains black hole even in the limit. Secondly, as seen in Fig. 12, one has $N^2/S^2 \sim r$ for $r \leq 0.5$ for a solution with a very small r_H . However, one has $S = \sqrt{1 - r_H/r} \rightarrow 1$ as $r_H \rightarrow 0$, hence one has in this limit $N^2 \sim r$ and the limiting form of the g-metric is something like a “zero size black hole”. The numerical profiles shown in Fig. 12 suggest this limiting configuration to have the following structure at small r :

$$N^2 \sim Y^2 \sim Q^2 \sim q^2 \sim r, \quad U = U_{\min} + \mathcal{O}(r). \quad (11.7)$$

The g-geometry is singular since its Ricci invariant $R(g) = 2/r^2 + \mathcal{O}(1/r)$ at small r , but the f-geometry remains of the regular black hole type because U does not vanish. Curiously, the temperature remains finite for $r_H \rightarrow 0$ and is always the same for both metrics. The limiting g-temperature can be formally computed by assuming $N^2 = \alpha r$, $Q^2 = \beta r$ with $\alpha \approx 0.7$ and $\beta \approx 6$ from Fig. 12. Eq.(6.5) then yields $T = \sqrt{\alpha\beta}/(4\pi) \approx 0.163$, which is very close to the value $T = 0.16$ for the solution with $r_H \sim 10^{-5}$ shown in Fig. 12. However, these considerations are of course purely formal since the zero size black hole cannot evaporate and further reduce its size, and the standard WKB arguments for the black hole evaporation do not apply because the geometry is singular at the horizon.

B. The “tachyon limit” $r_H \rightarrow r_H^{\max}(\eta)$

In this limit the solutions always remain regular and disappear after the fusion of roots of the algebraic equation (6.3) (or (A.8)). As explained above, this equation determines the horizon values of the solutions. Its two roots determine two solution branches, but only the root with $\sigma = +1$ gives rise to asymptotically flat solutions, the other branch showing a singularity of the g-metric outside the horizon. When r_H increases, the determinant of (6.3) decreases and vanishes for some $r_H = r_H^{\text{tach}}(\eta)$, then it becomes positive again, decreases again and vanishes for the second time for $r_H = r_H^{\max}(\eta) > r_H^{\text{tach}}(\eta)$, after which it becomes negative and the procedure stops. Specifically, it turns out that the determinant of (6.3) factorizes,

$$\mathcal{D} \equiv \mathcal{B}^2 - 4\mathcal{AC} = \mathcal{P}_1^2(r_H) D \quad \Rightarrow \quad \sqrt{\mathcal{D}} = \mathcal{P}_1(r_H)\sqrt{D}, \quad (11.8)$$

where $\mathcal{P}_1(r_H)$ is defined by (3.5) with $\mathbf{u} = U/r$ replaced by $u = U_H/r_H$ while D is a complicated function of r_H, U_H, η, c_3, c_4 . When r_H increases, then $\mathcal{P}_1(r_H)$ crosses zero at some $r_H = r_H^{\text{tach}}(\eta)$ while D remains positive, hence the square root \sqrt{D} changes sign. When r_H continues to increase, then D approaches zero and vanishes as $r_H \rightarrow r_H^{\text{max}}(\eta)$. No further increase of r_H is possible since D would then be negative thus rendering the solutions complex-valued.

Although the determinant \mathcal{D} vanishes for $r_H = r_H^{\text{tach}}(\eta)$ when $\mathcal{P}_1(r_H) = 0$ and also for $r_H = r_H^{\text{max}}(\eta)$ when $D = 0$, the two solution branches never merge. Specifically, the two horizon values ν_H determined by (A.8) merge when $\mathcal{D} = 0$, but a careful inspection reveals that y_H, U_H in (A.5), (A.6) remain different for the two branches when $\mathcal{P}_1(r_H) = 0$. If $D = 0$ then all horizon values ν_H, y_H, U_H coincide for the two branches, but the derivatives y'_H defined by (A.12) remain different. This is a consequence of the fact that the existence and uniqueness theorem applies only to regular points of the differential equations, whereas the event horizon $r = r_H$ is a singular point.

In the interval $r_H^{\text{tach}}(\eta) < r_H < r_H^{\text{max}}(\eta)$ the solutions show a “tachyon zone” near the horizon where the function $\mathcal{P}_1(r)$ defined by (3.5) is negative, as shown on the right panel in Fig. 12. Let us remember relation (2.13) for the Fierz-Pauli mass of gravitons obtained via linearizing the field equations around flat background. This relation can be written as $m_{\text{FP}}^2 = \mathcal{P}_1(\infty) m^2$. However, the equations can be similarly linearized around an arbitrary background solution, which yields in the spherically symmetric case the position-dependent mass term [61]

$$m_{\text{FP}}^2 = \mathcal{P}_1(r) m^2. \quad (11.9)$$

Therefore, if $\mathcal{P}_1(r) < 0$ then the mass effectively becomes imaginary. As a result, solutions for $r_H > r_H^{\text{tach}}$ show unphysical features, hence we call $r_H \rightarrow r_H^{\text{max}}(\eta)$ “tachyon limit”. The horizon value y'_H diverges in this limit, but this seems to be an integrable divergence similar to $y'(r) \sim 1/\sqrt{r - r_H}$ and the limiting solution itself stays regular. We were able to approach this solution rather closely, as shown in Fig. 12 (right panel) which presents “an almost limiting” solution with the horizon value of the determinant $D \sim 10^{-6}$.

To recapitulate, regular solutions exist only within a finite range of the event horizon radius, for $r_H^{\text{min}}(\eta) < r_H \leq r_H^{\text{max}}(\eta)$.

C. The ADM mass

What is important, is that the ADM mass also varies within a finite range. It seems this fact was not recognised in Ref. [44], which always shows only the normalized mass M/M_S with $M_S = r_H/2$, and this diverges as $r_H \rightarrow 0$. However, the mass M remains finite. As seen

in Fig. 11, the mass of all solutions, even of those with $r_H \rightarrow 0$, is actually bounded by the limiting values of the mass of the $\eta = \pi/2$ solutions,

$$\frac{1}{2} r_H^{\min}(\eta = \pi/2) \approx 0.23 < M < \frac{1}{2} r_H^{\max}(\eta = \pi/2) \approx 0.52. \quad (11.10)$$

In other words, the mass can be neither very small nor very large and is always close to the mass of the Schwarzschild solution with $r_H = 0.86$,

$$M \sim \frac{0.86}{2} = 0.43. \quad (11.11)$$

This means that the dimensionful mass

$$M = \frac{8\pi M}{m L_{\text{Pl}}} M_{\text{Pl}} \quad (11.12)$$

is always close to that of the Schwarzschild black hole of size $r_H = 0.86/m$, which is close to the Compton length of massive gravitons. As a result, one cannot assume the graviton mass m to be very small and of the order of the inverse Hubble radius as in (5.5). Indeed, this would imply the hairy black holes to be as heavy as the Schwarzschild black hole of a cosmological size – a physically meaningless result. However, assuming instead that $1/m \sim 10^6$ km as in (5.7), which is consistent with the cosmological observations if κ_1 is parametrically small as expressed by (5.6), yields a physically acceptable result. The masses of the hairy black holes are then close to the mass of the Schwarzschild black hole of radius $\sim 10^6$ km, that is $\sim 10^6 M_\odot$. This is typical for supermassive astrophysical black holes observed in the center of many galaxies.

Therefore, if the massive bigravity theory indeed describes physics, the “hairy features” can be present only in supermassive black holes and not in black holes of a smaller mass.

D. Parameter regions for solutions with $c_3 = -c_4 = 5/2$

Let us now collect all the facts together. The diagram in Fig. 13 shows the region in the (r_H, η) plane within which there are regular hairy black hole solutions. The low boundary of this region at $\eta = 0$ corresponds to solutions whose f-metric is Schwarzschild, while the upper boundary at $\eta = \pi/2$ corresponds to solutions whose g-metric is Schwarzschild. The left boundary consists of two pieces – the curve separating the left upper corner where the solutions are singular because their f-metric shows additional zeroes, and the portion of the η -axes corresponding to the “zero size black holes”. Finally, the right boundary corresponds to the “tachyon limit” beyond which the solutions become complex-valued.

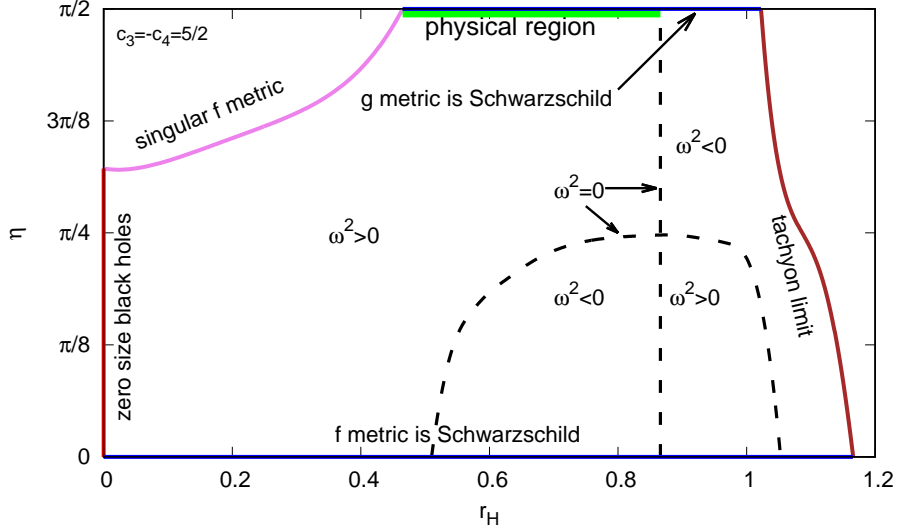


FIG. 13. The parameter region in the (r_H, η) plane corresponding to regular hairy black hole solutions with $c_3 = -c_4 = 5/2$. The dashed black $\omega^2 = 0$ lines separate stable and unstable sectors.

The diagram also shows lines corresponding to the zero modes, $\omega^2 = 0$, of the perturbative eigenvalue problem (10.6). The vertical line corresponds to the GL value $r_H = 0.86$. The eigenvalue ω^2 changes sign when crossing these lines, therefore, the lines separate sectors where $\omega^2 > 0$ and hence the solutions are stable, from sectors where $\omega^2 < 0$ and the solutions are unstable. There are altogether two stable and two unstable sectors. It is worth noting that the stability region is now much larger than for solutions with $c_3 = -c_4 = 2$ considered in the previous Section. One also notices that the tachyonic solutions are in the unstable sector.

Finally, the diagram shows the “physical region” corresponding to physically acceptable solutions. As explained above, for such solutions the coupling $\kappa_1 = \cos^2(\eta)$ should be very small for their mass not to be too large. Therefore, η should be very close to $\pi/2$. The solutions should be stable, hence they should correspond to the sector where $\omega^2 > 0$. These conditions specify the physical region to be the thick (green online) line at the top of the diagram.

Physical solutions are therefore described by the g-metric which is extremely close to Schwarzschild, since

$$G_{\mu\nu}(g) = \kappa_1 T_{\mu\nu}(g, f), \quad \text{where} \quad \kappa_1 \sim 10^{-34}. \quad (11.13)$$

The “hairy features” of the solutions hidden in the f-metric should be difficult to observe, unless in violent processes like black hole collisions producing large enough $T_{\mu\nu}(g, f)$ to overcome the 10^{-34} suppression. Summarizing, the static bigravity black holes should be extremely similar to the GR black holes, but their strong field dynamics is expected to be different.

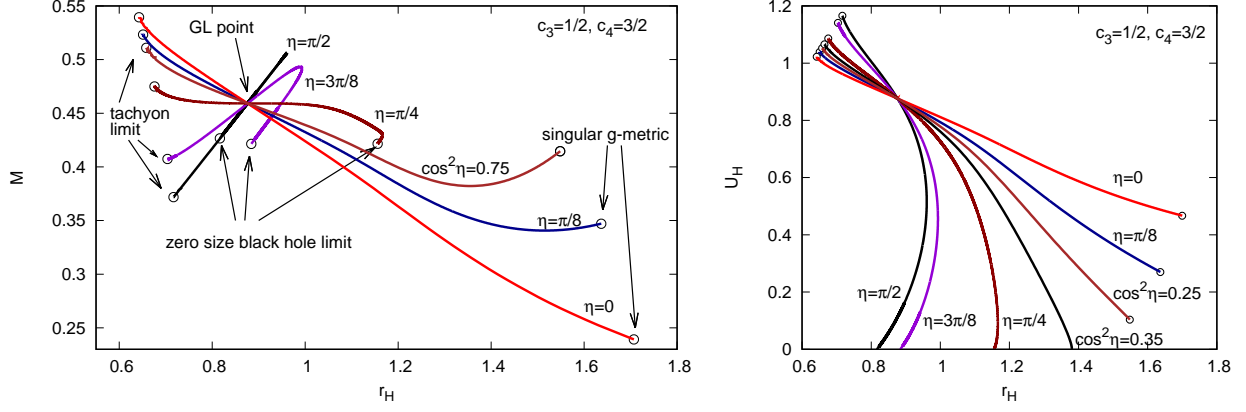


FIG. 14. The mass $M(r_H)$ (left) and the functions $U_H(r_H)$ (right) for the hairy black hole solutions with $c_3 = 1/2$, $c_4 = 3/2$.

E. Parameter regions for dual solutions with $c_3 = -1/2$, $c_4 = 3/2$

Let us now see how the described above solutions look after the duality transformation (9.10). This transformation converts the parameter values (11.1) into (11.2), flips the sign of $\eta - \pi/4$ and swaps the Q, N, r with q, Y, U . Graphically, this amounts to relabelling the functions and plotting them against U instead of r . The ADM mass and temperature are invariant under duality. The stability property also does not change since, for example, if a solution is unstable and admits growing in time perturbations, then its dual version will contain the same growing modes and hence will be unstable as well.

Fig. 14 shows the dual version of Fig. 11. The mass curves $M(r_H)$ still intersect in the GL point but they look quite different as compared to those in Fig. 11. In particular, not all of them are single valued. The reason is that the functions $U_H(r_H)$ in Fig. 11 are not always monotone, hence their inverses shown in Fig. 14 are not single-valued. As is seen on the right panel in Fig. 14, for each value of η such that $0 \leq \cos^2 \eta \leq 0.35$ there are two different solutions with the same r_H but with different U_H . As a result, the curves $M(r_H)$ are not always single valued.

The solutions still exist in a finite interval $r_H \in [r_H^{\min}(\eta), r_H^{\max}(\eta)]$, but the limits are now different. The lower limit $r_H^{\min}(\eta)$ can no longer extend down to zero but always corresponds to the tachyon solutions with vanishingly small horizon determinant D . The upper limit $r_H^{\max}(\eta)$ corresponds for small η to solutions whose g-metric (which used to be the f-metric before the duality) starts being singular. For larger values of η the upper limit $r_H^{\max}(\eta)$ corresponds rather to the point where the two different solutions with the same r_H but with different U_H merge to each other. The zero size black holes still exist but now correspond to internal points of

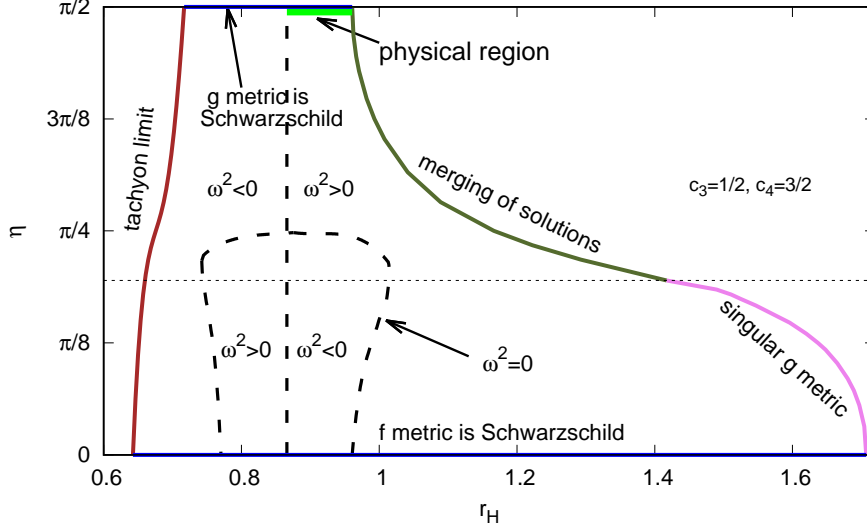


FIG. 15. The parameter region in the (r_H, η) plane corresponding to regular hairy black hole solutions with $c_3 = 1/2$, $c_4 = 3/2$. The dashed black $\omega^2 = 0$ lines separate stable and unstable sectors.

the interval $[r_H^{\min}(\eta), r_H^{\max}(\eta)]$.

We notice that the solutions below the GL point, for $r_H < 0.86$, are still more energetic than the solution with $\eta = \pi/2$, hence their “hair mass” M_{hair} is positive, whereas above the GL point it becomes negative. Finally, Fig. 15 shows the existence diagram in the (r_H, η) plane, together with the stability regions. The diagram looks quite different as compared to that in Fig. 11, although it corresponds to essentially the same solutions, up to the duality transformation. Although the duality does not change stability, it interchanges positions of the stability sectors. Therefore, the physical region corresponding to stable solutions with η close to $\pi/2$ is now above the GL point, where the hair mass is negative. The physical solutions are again characterised by the g-metric that is extremely close to Schwarzschild, but the novel feature is that now for each value of r_H from the physical region there are two different solutions whose g-metrics are almost the same but the f-metrics are different.

Although the described above features correspond to just two particular sets of values of c_3, c_4 , our numerics indicate that they are essentially generic. The solutions always exist only within a finite region of the (r_H, η) plane whose borders correspond to the tachyon limit, to the singular solutions, etc. The physical solutions always correspond to values of η very close to $\pi/2$ and to values of r_H close to the GL value $r_H = 0.86$. As a result, the hairy solutions always have the g-geometry close to that for the supermassive astrophysical black holes.

XII. Concluding remarks

To recapitulate, we presented above a detailed analysis of static and asymptotically flat black holes in the ghost-free massive bigravity theory. Extending the earlier result of [44], we find that for given values of the theory parameters c_3, c_4, η and for a given even horizon size within a finite range, $r_H \in [r_H^{\min}(\eta, c_3, c_4), r_H^{\max}(\eta, c_3, c_4)]$, there are one or sometimes two different black holes supporting a non-linear massive graviton hair, in addition to the trivial Schwarzschild solution with $g_{\mu\nu} = f_{\mu\nu}$. The hairy solutions are more energetic than the Schwarzschild one if $r_H < 0.86$, and they are less energetic otherwise. When r_H approaches the limiting values r_H^{\min} or r_H^{\max} , the solutions either become singular or complex valued or merge between themselves. Depending on values of r_H, c_3, c_4, η , the hairy solutions can be either stable or unstable.

The dimensionless ADM mass of the hairy solutions can be neither too large nor too small and is always not far from the GL value, $M = 0.43$. Therefore, to avoid the hairy black holes being unphysically heavy, one is bound to assume the massive graviton Compton length to be of the order of 10^6 km, in which case the agreement with the cosmological data is achieved by assuming that $\cos^2 \eta \sim (M_{\text{ew}}/M_{\text{Pl}})^2 \sim 10^{-34}$. The stable hairy black holes are then described by the g-metric which is extremely close to the Schwarzschild metric, although the f-metric is different, and they have the size and mass close to those of ordinary black holes of mass $M \sim 10^6 M_\odot$. As a result, if the bigravity theory indeed applies to describe physics, the supermassive astrophysical black holes should hide inside the “hairy features”, which should become manifest in violent processes like black hole collisions.

Finally, we should discuss the paper [45] that also considers black holes in the ghost-free massive bigravity theory. This paper presents essentially the same classification of different types of black holes as the one previously given in [18] but in a more refined way, extending it and paying attention to some subtle points. The paper addresses in particular the issue of convergence of the solutions to the flat background in the asymptotic region. Among other things, it claims that the Schwarzschild solution is the only asymptotically flat black hole in the theory. At the same time, the paper does not contain a rigorous proof of this statement but gives just a number of plausibility arguments, so that the claim should rather be viewed as a conjecture, as actually explicitly stated in some places of [45]. These arguments are as follows.

First of all, it was emphasised in [45] that the usual practice of starting the numerical integration not at the horizon $r = r_H$, which is a singular point of the differential equations,

but at a regular nearby point $r = r_H + \epsilon$, as was done in [44], could in principle lead to numerical instabilities. We agree with this, and it is for this reason that we use the desingularization procedure (described in Appendix A below) which allows us to start the numerical integration exactly at $r = r_H$ (initial conditions exactly at $r = r_H$ were described also in [45]).

The paper [45] makes also another remark concerning the behaviour at the horizon. It is known that in order to be able to *cross* the horizon, for example when studying geodesics, one cannot use the Schwarzschild coordinates and one should introduce instead regular at the horizon coordinates. These can be, for example, Eddington-Finkelstein (EF) coordinates in which $g_{00} = g_{11} = 0$, $g_{01} = g_{10} \neq 0$. It was noticed in [45] that the f-metric, when expressed in the same coordinates, generically does not have the same form, since it has $f_{11} \neq 0$, hence the two metrics cannot be simultaneously EF. We understand this, but this does not invalidate the background solutions (Ref. [45] agrees on this). The horizon geometries are regular, and if one wishes, one can use the same boundary conditions at the horizon to integrate inside the horizon to recover the interior solutions. Within the parametrization described in Appendix A, this is achieved by simply changing the sign of the numerical integration step.

Next, small initial deviations from the Schwarzschild solution via setting at the horizon $u = U_H/r_H = 1 + \epsilon$ were considered in [45]. Integrating the equations toward large r then yields metrics whose components diverge as $r \rightarrow \infty$ instead of approaching finite values. In addition, they show curvature singularities at a finite r where the amplitudes q, Y, U' change sign. This observation, made already in [18], shows that there are no regular and asymptotically flat solutions *in a small vicinity* of the Schwarzschild solution. However, there can be regular solutions corresponding to u considerably deviating from unit value.

Finally, the paper [45] reproduces and analyzes (in Appendix A) one of the asymptotically flat solution found in [44]. It chooses for this a *singular* solution with oscillating q, Y, U' amplitudes – in order to illustrate the pathologies that may arise. The regular solutions are not specially considered in [45] because, within the numerical approach adopted in that work, they also look pathological. Specifically, Appendix D of [45] describes the numerical method – a straightforward integration starting from the horizon with the standard routine of MATHEMATICA. This adequately produces the solution with a given precision, but only within a finite range of the radial coordinate r . If one integrates farther trying to approach flat space, then the growing mode Ce^{+r} generically present in the solution leads to a rapid accumulation of numerical errors triggering a numerical instability. Trying to suppress this mode by adjusting the horizon boundary conditions, one typically observes the derivatives of some functions in the solution growing without bounds at some finite r . Precisely this type of

behaviour at the end of the integration interval is seen in Fig.11 in [45].

Therefore, one cannot get asymptotically flat solutions within the numerical scheme adopted in [45], since pathological features arise in this scheme inevitably. This must be the reason behind the conviction that such solutions do not exist. However, all pathologies can be eliminated within the more elaborate numerical scheme described above – via suppressing the growing Ce^{+r} mode from the very beginning.

Acknowledgments.— We thank Francesco Torsello, Mikica Kocic and Edvard Mörtzell for clarifying discussions and useful remarks. The work of M.S.V. was partly supported by the French National Center of Scientific Research within the collaborative French-Russian research program, Grant No. 289860, as well as by the Institute of Theoretical and Mathematical Physics at the Moscow University during the visit in the early 2020, and also by the Russian Government Program of Competitive Growth of the Kazan Federal University.

Appendix

In the following two appendices we describe the desingularization procedure and the time-dependent case.

A. Desingularization at the horizon

The horizon $r = r_H$ is a singular point of the differential equations – the derivatives N' and Y' expressed by Eqs.(4.23) are not defined at this point. The usual practice to handle this difficulty is to use the local power series expansions (6.1),(6.2) to start the numerical integration not exactly at $r = r_H$ but at a nearby point with $r = r_H + \epsilon$ where ϵ is a small number. One may then hope that the results will not be very sensitive to the value of ϵ . However, in such an approach ϵ remains an arbitrary parameter not defined by any prescription. This inevitably affects the stability of the numerical procedure, which becomes evident when one studies the dependence of the solutions on the theory parameters.

At the same time, it is possible to reformulate the problem in such a way that the numerical integration starts exactly at $r = r_H$. Let us make the change of variables

$$N = S \nu, \quad Y = S y \quad \text{with} \quad S = \sqrt{1 - \frac{r_H}{r}}. \quad (\text{A.1})$$

The functions ν, y and their derivatives are defined also at $r = r_H$. Eqs.(4.3),(4.4) then yield

$$\nu' = -\frac{\nu}{2r} + \frac{\mathcal{C}_1}{2\nu y r^2 S^2}, \quad y' = -\frac{y U'}{2U} + \frac{\mathcal{C}_2}{2\nu y r^2 U S^2}, \quad (\text{A.2})$$

where

$$\begin{aligned}\mathcal{C}_1 &= (r - r_H \nu^2 - \kappa_1 r^3 \mathcal{P}_0) y - \kappa_1 r^3 \mathcal{P}_1 U' \nu, \\ \mathcal{C}_2 &= \nu r^2 (1 - \kappa_2 r^2 \mathcal{P}_2) U' - \kappa_2 r^4 \mathcal{P}_1 y - r_H U \nu y^2.\end{aligned}\quad (\text{A.3})$$

At the horizon the derivatives ν' and y' are finite, which requires that

$$\mathcal{C}_{1|_{r_H}} = 0, \quad \mathcal{C}_{2|_{r_H}} = 0, \quad (\text{A.4})$$

from where one obtains the horizon values

$$U'_H = \frac{(1 - \nu^2 - \kappa_1 r^2 \mathcal{P}_0) y}{\kappa_1 r^2 \mathcal{P}_1 \nu} \Big|_{r_H}, \quad (\text{A.5})$$

$$y_H = \frac{1 + (\kappa_2 r^2 \mathcal{P}_2 - 1) \nu^2 + \kappa_1 \kappa_2 (\mathcal{P}_0 \mathcal{P}_2 - \mathcal{P}_1^2) r^4 - (\kappa_1 \mathcal{P}_0 + \kappa_2 \mathcal{P}_2) r^2}{\kappa_1 r \mathcal{P}_1 U \nu} \Big|_{r_H}. \quad (\text{A.6})$$

At the same time, the horizon value of U' can be obtained from (4.23),

$$U'_H = \lim_{r \rightarrow r_H} \mathcal{D}_U(r, U, S\nu, Sy) \equiv \mathcal{D}_{UH}(r_H, U_H, \nu_H, y_H). \quad (\text{A.7})$$

This value must agree with the one given by (A.5), which yields a condition on ν_H , and using (A.6), this condition reduces (if β_k are chosen according to (2.15)) to a biquadratic equation

$$\mathcal{A}(\nu_H^2)^2 + \mathcal{B}\nu_H^2 + \mathcal{C} = 0, \quad (\text{A.8})$$

where the coefficients \mathcal{A} , \mathcal{B} , \mathcal{C} are (rather complicated) functions of r_H, U_H . As a result, for given r_H, U_H there are two possible horizon values $\nu_H^{(1)}$ and $\nu_H^{(2)}$. Injecting to (A.5) and (A.6), this determines the horizon values y_H and U'_H . Finally, the horizon values of ν' and y' are obtained from (A.2) by taking the $S \rightarrow 0$ limit and using the l'hospital's rule, which yields

$$\nu'_H = -\frac{\nu_H}{2r_H} + \frac{\mathcal{C}'_{1|_{r_H}}}{2r_H \nu_H y_H}, \quad y'_H = -\frac{y_H U'_H}{2U_H} + \frac{\mathcal{C}'_{2|_{r_H}}}{2r_H \nu_H y_H U_H}. \quad (\text{A.9})$$

There remains to compute the derivatives here. One has, for example,

$$\mathcal{C}'_{1|_{r_H}} = \left(\frac{\partial}{\partial r} + \nu'_H \frac{\partial}{\partial \nu} + y'_H \frac{\partial}{\partial y} + U'_H \frac{\partial}{\partial U} + U''_H \frac{\partial}{\partial U'} \right) \mathcal{C}_1(r, U, \nu, y, U') \Big|_{r=r_H, U=U_H, \nu=\nu_H, y=y_H} \quad (\text{A.10})$$

where the second derivative is similarly obtained from (A.7),

$$U''_H = \left(\frac{\partial}{\partial r} + \nu'_H \frac{\partial}{\partial \nu} + y'_H \frac{\partial}{\partial y} + U'_H \frac{\partial}{\partial U} \right) \mathcal{D}_U(r, U, S\nu, Sy) \Big|_{r=r_H, U=U_H, \nu=\nu_H, y=y_H}, \quad (\text{A.11})$$

and similar expressions for $\mathcal{C}'_{2|_{r_H}}$. Injecting this to (A.9) yields *linear* in ν'_H and y'_H relations, which can be resolved to give (we do not show explicit formulas in view of their complexity)

$$\nu'_H = \nu'_H(r_H, U_H, \nu_H, y_H), \quad y'_H = y'_H(r_H, U_H, \nu_H, y_H). \quad (\text{A.12})$$

Summarizing the above discussion, the equations in the desingularized form read

$$\begin{aligned}\nu' &= -\frac{\nu}{2r} + \frac{\mathcal{C}_1}{2\nu y r^2 S^2} \equiv \mathcal{F}_\nu(r, U, \nu, y), \\ y' &= -\frac{yU'}{2U} + \frac{\mathcal{C}_2}{2\nu y r^2 U S^2} \equiv \mathcal{F}_y(r, U, \nu, y), \\ U' &= \mathcal{D}_U(r, U, S\nu, Sy) \equiv \mathcal{F}_U(r, U, \nu, y),\end{aligned}\tag{A.13}$$

where \mathcal{C}_1 and \mathcal{C}_2 are defined by (A.3) while \mathcal{D}_U is the same as in (4.23). These equations apply for $r > r_H$, while at $r = r_H$ they should be replaced by

$$\begin{aligned}\nu' &= \nu'_H(r_H, U_H, \nu_H, y_H), \\ y' &= y'_H(r_H, U_H, \nu_H, y_H), \\ U' &= U'_H(r_H, U_H, \nu_H, y_H),\end{aligned}\tag{A.14}$$

where ν'_H , y'_H , U'_H are defined by Eqs.(A.5),(A.12). The horizon values r_H and $U_H \equiv ur_H$ can be arbitrary, while ν_H is not arbitrary but must fulfil the algebraic equation (A.8), whereas y_H is determined by (A.6). This formulation allows one to start the integration exactly at the horizon $r = r_H$ and then continue to the $r > r_H$ region.

B. Field equations with time dependance

Let us allow both metrics to depend on time, assuming that they are still spherically symmetric. The gauge freedom of reparametrizations of the t, r coordinates can be used to make the g-metric diagonal, but the f-metric will in general contain an off-diagonal term. The two metrics can be written as [10]

$$\begin{aligned}ds_g^2 &= -Q^2 dt^2 + \frac{dr^2}{\Delta^2} + R^2 d\Omega^2, \\ ds_f^2 &= -(q^2 - \alpha^2 Q^2 \Delta^2) dt^2 - 2\alpha \left(q + \frac{Q\Delta}{W} \right) dt dr + \left(\frac{1}{W^2} - \alpha^2 \right) dr^2 + U^2 d\Omega^2,\end{aligned}\tag{B.1}$$

where $d\Omega^2 = d\theta^2 + \sin^2 \theta d\phi^2$ and $Q, q, \Delta, W, \alpha, U, R$ are functions of r and t .

One can check that the tensor

$$\gamma^\mu{}_\nu = \begin{pmatrix} q/Q & \alpha/Q & 0 & 0 \\ -\alpha Q \Delta^2 & \Delta/W & 0 & 0 \\ 0 & 0 & U/R & 0 \\ 0 & 0 & 0 & U/R \end{pmatrix}\tag{B.2}$$

has the property $\gamma^\mu{}_\sigma \gamma^\sigma{}_\nu = g^\mu{}_\sigma f^\sigma{}_\nu$. This tensor is used to compute the energy-momentum tensors $T^\mu{}_\nu$ and $\mathcal{T}^\mu{}_\nu$ in (2.7).

One can redefine the two amplitudes similarly to (4.1)

$$N = \Delta R', \quad Y = WU', \quad (\text{B.3})$$

where the prime denotes the derivative with respect to r , and one can impose the gauge condition

$$R = r. \quad (\text{B.4})$$

As a result, the independent field equations (2.18) become

$$\begin{aligned} G_0^0(g) &= \kappa_1 T_0^0, & G_1^1(g) &= \kappa_1 T_1^1, & G_1^0(g) &= \kappa_1 T_1^0, \\ G_0^0(f) &= \kappa_2 \mathcal{T}_0^0, & G_1^1(f) &= \kappa_2 \mathcal{T}_1^1, & G_1^0(f) &= \kappa_2 \mathcal{T}_1^0, \end{aligned} \quad (\text{B.5})$$

plus two non-trivial components of the the conservation condition $\overset{(g)}{\nabla}_\mu T^\mu_\nu = 0$,

$$\overset{(g)}{\nabla}_\mu T^\mu_0 = 0, \quad \overset{(g)}{\nabla}_\mu T^\mu_1 = 0. \quad (\text{B.6})$$

Here one has explicitly

$$G(g)_0^0 = \frac{N^2 - 1}{r^2} + \frac{2NN'}{r}, \quad G_1^1(g) = \frac{N^2 - 1}{r^2} + \frac{2N^2 Q'}{rQ}, \quad G_1^0(g) = \frac{2\dot{N}}{rNQ^2}, \quad (\text{B.7})$$

where the dot denotes the partial derivative with respect to t , while

$$T_0^0 = -\mathcal{P}_0 - \mathcal{P}_1 \frac{NU'}{Y}, \quad T_1^1 = -\mathcal{P}_0 - \mathcal{P}_1 \frac{q}{Q}, \quad T_1^0 = \mathcal{P}_1 \frac{\alpha}{Q}, \quad (\text{B.8})$$

where \mathcal{P}_m are defined in (3.5). The components of the second stress-energy tensor are

$$\begin{aligned} \mathcal{T}_0^0 &= -\frac{r^2}{NU^2 \mathcal{A}} \left(\mathcal{P}_1 qY + \mathcal{P}_2 (\alpha^2 N^2 QY + qNU') \right), \\ \mathcal{T}_1^1 &= -\frac{r^2}{U^2 \mathcal{A}} \left(\mathcal{P}_1 QU' + \mathcal{P}_2 (\alpha^2 NQY + qU') \right), \\ \mathcal{T}_1^0 &= -\frac{r^2}{NU^2 \mathcal{A}} \mathcal{P}_1 Y \alpha, \end{aligned} \quad (\text{B.9})$$

where $\mathcal{A} = NQY\alpha^2 + qU'$. The components of the Einstein tensor for $f_{\mu\nu}$, are complicated:

$$\begin{aligned}
G(f)^0_0 = & -\frac{1}{U^2Y\mathcal{A}^3} \left(N^3Q^3Y^4\alpha^6 + (-NQ\dot{U}^2Y^4 + N^3Q^3U'^2Y^4 + 2N^3Q^3UU''Y^4 \right. \\
& + 3N^2qQ^2U'Y^3)\alpha^4 + (-2NQU\dot{U}\dot{\alpha}Y^4 - 2qQU\dot{U}N'Y^4 + 2NQU\dot{U}q'Y^4 \\
& - 2NqU\dot{U}Q'Y^4 + 2NqQ\dot{U}U'Y^4 - 2N^3Q^3UU'\alpha'Y^4 + 2NqQU\dot{U}'Y^4 \\
& + 2N^2Q^2\dot{U}U'^2Y^3 + 2N^2Q^2UU'\dot{U}'Y^3 + 2N^2Q^2U\dot{U}U''Y^3 - 2N^2Q^2U\dot{U}U'Y'Y^2)\alpha^3 \\
& + (-Nq^2QU'^2Y^4 + 2q^2QU\dot{U}N'U'Y^4 - 2NqQUq'U'Y^4 + 2Nq^2UQ'U'Y^4 \\
& - 2NqQU\dot{U}\alpha'Y^4 - 2Nq^2QUU''Y^4 + N^2qQ^2U'^3Y^3 + 2NqQ^2UN'U'^2Y^3 \\
& - 2N^2Q^2Uq'U'^2Y^3 + 2N^2qQUQ'U'^2Y^3 - q\dot{U}^2U'Y^3 - 2N^2Q^2U\dot{U}U'\alpha'Y^3 \\
& + NQ\dot{U}^2U'^2Y^2 + 3Nq^2QU'^2Y^2 + 2N^2qQ^2UU'^2Y'Y^2 + 2NQU\dot{U}U'\dot{U}'Y^2 \\
& - 2NQU\dot{U}\dot{Y}'U'^2Y)\alpha^2 + (4Nq^2QUU'\alpha'Y^4 + 2q^2\dot{U}U'^2Y^3 - 2qU\dot{U}\dot{\alpha}U'Y^3 \\
& + 2N^2qQ^2UU'^2\alpha'Y^3 + 2q^2UU'\dot{U}'Y^3 - 2q^2U\dot{U}U''Y^3 + 2NqQ\dot{U}U'^3Y^2 \\
& + 2qQU\dot{U}N'U'^2Y^2 - 2NQU\dot{U}q'U'^2Y^2 + 2NqU\dot{U}Q'U'^2Y^2 + 2q^2U\dot{U}U'Y'Y^2 \\
& + 2NqQUU'^2\dot{U}'Y^2)\alpha - q^3Y^3U'^3 + qY\dot{U}^2U'^3 + q^3YU'^3 - 2qU\dot{U}\dot{Y}'U'^3 \\
& \left. - 2q^3UY^2U'^2Y' + 2NqQUY^2\dot{U}U'^2\alpha' + 2q^2UY^3\dot{U}U'\alpha' + 2qUY\dot{U}U'^2\dot{U}' \right),
\end{aligned}$$

$$\begin{aligned}
G(f)^0_1 = & -\frac{2}{UY\mathcal{A}^3} \left((-Q\dot{U}N'Y^4 - N\dot{U}Q'Y^4 + NQ\dot{U}'Y^4)\alpha^4 + (-NQ\dot{\alpha}U'Y^4 \right. \\
& + qQN'U'Y^4 + NqQ'U'Y^4 - NQ\dot{U}\alpha'Y^4 - NqQU''Y^4 + NQ^2N'U'^2Y^3 \\
& + N^2QQ'U'^2Y^3 - N^2Q^2U'U''Y^3)\alpha^3 + (2NqQU'\alpha'Y^4 - \dot{U}q'U'Y^3 + qU'\dot{U}'Y^3 \\
& + 2N^2Q^2U'^2\alpha'Y^3 - q\dot{U}U''Y^3 + Q\dot{U}N'U'^2Y^2 + N\dot{U}Q'U'^2Y^2 + q\dot{U}U'Y'Y^2 \\
& - NQ\dot{U}U'U''Y^2 - NQ\dot{Y}'U'^3Y + NQ\dot{U}U'^2Y'Y)\alpha^2 + (-q\dot{\alpha}U'^2Y^3 + qq'U'^2Y^3 \\
& + q\dot{U}U'\alpha'Y^3 + NQq'U'^3Y^2 - q^2U'^2Y'Y^2 + 2NQ\dot{U}U'^2\alpha'Y^2 - NqQU'^3Y'Y)\alpha \\
& \left. - q\dot{Y}'U'^4 + Y\dot{U}q'U'^3 \right),
\end{aligned}$$

$$\begin{aligned}
G(f)^1_1 = & -\frac{1}{U^2 \mathcal{A}^3} \left(N^3 Q^3 Y^3 \alpha^6 + (-NQ\dot{U}^2 Y^3 + N^3 Q^3 U'^2 Y^3 + 2QU\dot{N}\dot{U}Y^3 + 2NU\dot{Q}\dot{U}Y^3 \right. \\
& - 2NQU\ddot{U}Y^3 + 2N^2 Q^3 UN'U'Y^3 + 2N^3 Q^2 UQ'U'Y^3 + 3N^2 qQ^2 U'Y^2) \alpha^4 \\
& + (2NQU\dot{U}\dot{\alpha}Y^3 - 2qQU\dot{N}U'Y^3 + 2NQU\dot{q}U'Y^3 - 2NqU\dot{Q}U'Y^3 \\
& + 2NqQ\dot{U}U'Y^3 + 2N^3 Q^3 UU'\alpha'Y^3 + 2NqQU\dot{U}'Y^3 + 2N^2 Q^2 \dot{U}U'^2 Y^2 \\
& + 4N^2 Q^2 UU'\dot{U}'Y^2 - 2N^2 Q^2 U\dot{Y}U'^2 Y) \alpha^3 + (-Nq^2 QU'^2 Y^3 - 2NqQU\dot{\alpha}U'Y^3 \\
& - 2NqQUq'U'Y^3 + N^2 qQ^2 U'^3 Y^2 - 2N^2 Q^2 U\dot{\alpha}U'^2 Y^2 + 2NqQ^2 UN'U'^2 Y^2 \\
& + 2N^2 qQUQ'U'^2 Y^2 - q\dot{U}^2 U'Y^2 + 2U\dot{q}\dot{U}U'Y^2 - 2qU\ddot{U}U'Y^2 + 2qU\dot{U}\dot{U}'Y^2 \\
& + NQ\dot{U}^2 U'^2 Y + 3Nq^2 QU'^2 Y - 2QU\dot{N}\dot{U}U'^2 Y - 2NU\dot{Q}\dot{U}U'^2 Y + 2NQU\ddot{U}U'^2 Y \\
& - 2qU\dot{U}\dot{Y}U'Y + 2NQU\dot{U}U'\dot{U}'Y - 2NQU\dot{U}\dot{Y}U'^2) \alpha^2 + (2qQUY\dot{N}U'^3 \\
& - 2NQUY\dot{q}U'^3 + 2NqUY\dot{Q}U'^3 + 2NqQY\dot{U}U'^3 + 2q^2 Y^2 \dot{U}U'^2 + 2q^2 UY\dot{Y}U'^2 \\
& - 4NQUY\dot{U}\dot{\alpha}U'^2 + 2N^2 qQ^2 UY^2 \alpha'U'^2 + 2NqQUY\dot{U}'U'^2 - 2qUY^2 \dot{U}\dot{\alpha}U') \alpha \\
& + q^3 U'^3 - q^3 Y^2 U'^3 + q\dot{U}^2 U'^3 - 2U\dot{q}\dot{U}U'^3 + 2NqQUY\dot{\alpha}U'^3 + 2qU\ddot{U}U'^3 \\
& \left. + 2q^2 UY^2 \dot{\alpha}U'^2 - 2q^2 UY^2 q'U'^2 \right). \tag{B.10}
\end{aligned}$$

Finally, there are two non-trivial components of the conservation law,

$$\begin{aligned}
\stackrel{(g)}{\nabla}_\mu T^\mu_0 = & -\mathcal{P}_1 \left(\alpha N' NQ + 2\alpha N^2 Q + \alpha' N^2 Q + \frac{q\dot{N}}{NQ} + \frac{N\dot{U}'}{Y} - \frac{NU'\dot{Y}}{Y^2} \right) \\
& - \frac{d\mathcal{P}_0}{r} \left(\alpha N^2 Q + \dot{U} \right) - \frac{d\mathcal{P}_1}{r} \left(\alpha N^2 QU' + \frac{N\dot{U}U'}{Y} \right), \\
\stackrel{(g)}{\nabla}_\mu T^\mu_1 = & \mathcal{P}_1 \left(\frac{\dot{\alpha}}{Q} - \frac{\alpha\dot{N}}{NQ} - \frac{q'}{Q} + \frac{NQ'U'}{QY} \right) + \frac{d\mathcal{P}_1}{r} \left(\alpha^2 N^2 + \frac{\alpha\dot{U}}{Q} + \frac{qNU'}{QY} - \frac{qU'}{Q} \right) \\
& + \frac{d\mathcal{P}_0}{r} \left(\frac{NU'}{Y} - U' \right), \tag{B.11}
\end{aligned}$$

where $d\mathcal{P}_m$ are defined in (4.10). Eqs.(B.5), (B.6) comprise a system of 8 equations for 6 functions Q , q , Δ , W , α , U . For this system not to be overdetermined, only 6 equations out of 8 should be independent. As shown in Section X, this indeed happens at least for small α , when the perturbative analysis of the equations shows that some of them coincide.

-
- [1] A. Riess *et al.*, *Observational evidence from supernovae for an accelerating universe and a cosmological constant*, *Astron.Journ.* **116** (1998), no. 3 1009.
- [2] S. Perlmutter *et al.*, *Measurements of ω and λ from 42 high-redshift supernovae*, *Astrophys.Journ.* **517** (1999), no. 2 565.

- [3] M. Fierz and W. Pauli, *On relativistic wave equations for particles of arbitrary spin in an electromagnetic field*, *Proc.Roy.Soc.Lond.* **A173** (1939) 211–232, [[doi:10.1098/rspa.1939.0140](https://doi.org/10.1098/rspa.1939.0140)].
- [4] H. van Dam and M. J. G. Veltman, *Massive and massless Yang-Mills and gravitational fields*, *Nucl. Phys.* **B22** (1970) 397–411, [[doi:10.1016/0550-3213\(70\)90416-5](https://doi.org/10.1016/0550-3213(70)90416-5)].
- [5] V. I. Zakharov, *Linearized gravitation theory and the graviton mass*, *JETP Lett.* **12** (1970) 312.
- [6] A. I. Vainshtein, *To the problem of nonvanishing gravitation mass*, *Phys.Lett.* **B39** (1972) 393–394, [[doi:10.1016/0370-2693\(72\)90147-5](https://doi.org/10.1016/0370-2693(72)90147-5)].
- [7] D. G. Boulware and S. Deser, *Can gravitation have a finite range?*, *Phys.Rev.* **D6** (1972) 3368–3382, [[doi:10.1103/PhysRevD.6.3368](https://doi.org/10.1103/PhysRevD.6.3368)].
- [8] C. de Rham, G. Gabadadze, and A. Tolley, *Resummation of massive gravity*, *Phys.Rev.Lett.* **106** (2011) 231101, [[arXiv:1011.1232](https://arxiv.org/abs/1011.1232)], [[doi:10.1103/PhysRevLett.106.231101](https://doi.org/10.1103/PhysRevLett.106.231101)].
- [9] S. F. Hassan and R. A. Rosen, *Bimetric Gravity from Ghost-free Massive Gravity*, *JHEP* **02** (2012) 126, [[arXiv:1109.3515](https://arxiv.org/abs/1109.3515)], [[doi:10.1007/JHEP02\(2012\)126](https://doi.org/10.1007/JHEP02(2012)126)].
- [10] M. Volkov, *Cosmological solutions with massive gravitons in the bigravity theory*, *JHEP* **1201** (2012) 035, [[arXiv:1110.6153](https://arxiv.org/abs/1110.6153)], [[doi:10.1007/JHEP01\(2012\)035](https://doi.org/10.1007/JHEP01(2012)035)].
- [11] M. von Strauss, A. Schmidt-May, J. Enander, E. Mortsell, and F. Hassan, *Cosmological solutions in bimetric gravity and their observational tests*, *JCAP* **1203** (2012) 042, [[arXiv:1111.1655](https://arxiv.org/abs/1111.1655)], [[doi:10.1088/1475-7516/2012/03/042](https://doi.org/10.1088/1475-7516/2012/03/042)].
- [12] D. Comelli, M. Crisostomi, F. Nesti, and L. Pilo, *FRW cosmology in ghost free massive gravity*, *JHEP* **1203** (2012) 067, [[arXiv:1111.1983](https://arxiv.org/abs/1111.1983)], [[doi:10.1007/JHEP06\(2012\)020](https://doi.org/10.1007/JHEP06(2012)020), [10.1007/JHEP03\(2012\)067](https://doi.org/10.1007/JHEP03(2012)067)].
- [13] Y. Akrami, S. Hassan, F. Könnig, A. Schmidt-May, and A. R. Solomon, *Bimetric gravity is cosmologically viable*, *Phys. Lett. B* **748** (2015) 37–44, [[arXiv:1503.07521](https://arxiv.org/abs/1503.07521)], [[doi:10.1016/j.physletb.2015.06.062](https://doi.org/10.1016/j.physletb.2015.06.062)].
- [14] E. Mortsell and J. Enander, *Scalar instabilities in bimetric gravity: The Vainshtein mechanism and structure formation*, *JCAP* **10** (2015) 044, [[arXiv:1506.04977](https://arxiv.org/abs/1506.04977)], [[doi:10.1088/1475-7516/2015/10/044](https://doi.org/10.1088/1475-7516/2015/10/044)].
- [15] K. Aoki, K.-i. Maeda, and R. Namba, *Stability of the Early Universe in Bigravity Theory*, *Phys. Rev. D* **92** (2015), no. 4 044054, [[arXiv:1506.04543](https://arxiv.org/abs/1506.04543)], [[doi:10.1103/PhysRevD.92.044054](https://doi.org/10.1103/PhysRevD.92.044054)].
- [16] M. Lüben, E. Mortsell, and A. Schmidt-May, *Bimetric cosmology is compatible with local tests of gravity*, *Class. Quant. Grav.* **37** (2020), no. 4 047001, [[arXiv:1812.08686](https://arxiv.org/abs/1812.08686)], [[doi:10.1088/1361-6382/ab4f9b](https://doi.org/10.1088/1361-6382/ab4f9b)].
- [17] M. Högås, F. Torsello, and E. Mortsell, *On the stability of bimetric structure formation*, *JCAP*

- 04 (2020) 046, [[arXiv:1910.01651](#)], [[doi:10.1088/1475-7516/2020/04/046](#)].
- [18] M. S. Volkov, *Hairy black holes in the ghost-free bigravity theory*, *Phys. Rev.* **D85** (2012) 124043, [[arXiv:1202.6682](#)], [[doi:10.1103/PhysRevD.85.124043](#)].
- [19] S. V. Sushkov and M. S. Volkov, *Giant wormholes in ghost-free bigravity theory*, *JCAP* **1506** (2015), no. 06 017, [[arXiv:1502.03712](#)], [[doi:10.1088/1475-7516/2015/06/017](#)].
- [20] M. Volkov, *Self-accelerating cosmologies and hairy black holes in ghost-free bigravity and massive gravity*, *Class.Quant.Grav.* **30** (2013) 184009, [[arXiv:1304.0238](#)], [[doi:10.1088/0264-9381/30/18/184009](#)].
- [21] C. Isham and D. Storey, *Exact Spherically Symmetric Classical Solutions for the F-G Theory of Gravity*, *Phys. Rev. D* **18** (1978) 1047, [[doi:10.1103/PhysRevD.18.1047](#)].
- [22] M. Gurses, *A new class of f-g fields relevant to quark confinement*, *Phys. Rev. D* **20** (1979) 1019–1021, [[doi:10.1103/PhysRevD.20.1019](#)].
- [23] M. Gurses, *Solutions of the f-g field equations*, *J. Phys. A* **14** (1981) 1957–1971, [[doi:10.1088/0305-4470/14/8/020](#)].
- [24] C. Isham, A. Salam, and J. Strathdee, *F-dominance of gravity*, *Phys.Rev.* **D3** (1971) 867–873, [[doi:10.1103/PhysRevD.3.867](#)].
- [25] E. Babichev and A. Fabbri, *Stability analysis of black holes in massive gravity: a unified treatment*, *Phys. Rev. D* **89** (2014), no. 8 081502, [[arXiv:1401.6871](#)], [[doi:10.1103/PhysRevD.89.081502](#)].
- [26] M. S. Volkov, *Hairy black holes in theories with massive gravitons*, *Lect. Notes Phys.* **892** (2015) 161–180, [[arXiv:1405.1742](#)], [[doi:10.1007/978-3-319-10070-8_6](#)].
- [27] Z. Berezhiani, D. Comelli, F. Nesti, and L. Pilo, *Exact Spherically Symmetric Solutions in Massive Gravity*, *JHEP* **07** (2008) 130, [[arXiv:0803.1687](#)], [[doi:10.1088/1126-6708/2008/07/130](#)].
- [28] D. Comelli, M. Crisostomi, F. Nesti, and L. Pilo, *Spherically Symmetric Solutions in Ghost-Free Massive Gravity*, *Phys. Rev. D* **85** (2012) 024044, [[arXiv:1110.4967](#)], [[doi:10.1103/PhysRevD.85.024044](#)].
- [29] E. Babichev and A. Fabbri, *A class of charged black hole solutions in massive (bi)gravity*, *JHEP* **07** (2014) 016, [[arXiv:1405.0581](#)], [[doi:10.1007/JHEP07\(2014\)016](#)].
- [30] E. Babichev and A. Fabbri, *Rotating black holes in massive gravity*, *Phys. Rev. D* **90** (2014) 084019, [[arXiv:1406.6096](#)], [[doi:10.1103/PhysRevD.90.084019](#)].
- [31] R. A. Rosen, *Black Hole Mechanics for Massive Gravitons*, *Phys. Rev. D* **98** (2018), no. 10 104008, [[arXiv:1805.12135](#)], [[doi:10.1103/PhysRevD.98.104008](#)].
- [32] E. Babichev, R. Brito, and P. Pani, *Linear stability of nonbidiagonal black holes in massive*

- gravity*, *Phys. Rev. D* **93** (2016), no. 4 044041, [[arXiv:1512.04058](#)], [[doi:10.1103/PhysRevD.93.044041](#)].
- [33] E. Babichev and A. Fabbri, *Instability of black holes in massive gravity*, *Class. Quant. Grav.* **30** (2013) 152001, [[arXiv:1304.5992](#)], [[doi:10.1088/0264-9381/30/15/152001](#)].
 - [34] M. S. Volkov and D. V. Galtsov, *NonAbelian Einstein Yang-Mills black holes*, *JETP Lett.* **50** (1989) 346–350. [*Pisma Zh. Eksp. Teor. Fiz.* 50,312(1989)].
 - [35] M. S. Volkov and D. V. Gal'tsov, *Gravitating nonAbelian solitons and black holes with Yang-Mills fields*, *Phys. Rept.* **319** (1999) 1–83, [[arXiv:hep-th/9810070](#)], [[doi:10.1016/S0370-1573\(99\)00010-1](#)].
 - [36] M. S. Volkov, *Hairy black holes in the XX-th and XXI-st centuries*, [arXiv:1601.08230](#).
 - [37] C. Deffayet and T. Jacobson, *On horizon structure of bimetric spacetimes*, *Class.Quant.Grav.* **29** (2012) 065009, [[arXiv:1107.4978](#)], [[doi:10.1088/0264-9381/29/6/065009](#)].
 - [38] M. Banados, A. Gomberoff, and M. Pino, *The bigravity black hole and its thermodynamics*, *Phys. Rev. D* **84** (2011) 104028, [[arXiv:1105.1172](#)], [[doi:10.1103/PhysRevD.84.104028](#)].
 - [39] W. Press, S. Teukolsky, W. Vetterling, and B. Flannery, *Numerical Recipes 3rd Edition: The Art of Scientific Computing*. Cambridge University Press, New York, NY, USA, 3 ed., 2007.
 - [40] J. Enander and E. Mortsell, *On stars, galaxies and black holes in massive bigravity*, *JCAP* **11** (2015) 023, [[arXiv:1507.00912](#)], [[doi:10.1088/1475-7516/2015/11/023](#)].
 - [41] K. Aoki, K.-i. Maeda, and M. Tanabe, *Relativistic stars in bigravity theory*, *Phys. Rev. D* **93** (2016), no. 6 064054, [[arXiv:1602.02227](#)], [[doi:10.1103/PhysRevD.93.064054](#)].
 - [42] R. Brito, V. Cardoso, and P. Pani, *Massive spin-2 fields on black hole spacetimes: Instability of the Schwarzschild and Kerr solutions and bounds on the graviton mass*, *Phys. Rev.* **D88** (2013), no. 2 023514, [[arXiv:1304.6725](#)], [[doi:10.1103/PhysRevD.88.023514](#)].
 - [43] R. Gregory and R. Laflamme, *Black strings and p-branes are unstable*, *Phys. Rev. Lett.* **70** (1993) 2837–2840, [[arXiv:hep-th/9301052](#)], [[doi:10.1103/PhysRevLett.70.2837](#)].
 - [44] R. Brito, V. Cardoso, and P. Pani, *Black holes with massive graviton hair*, *Phys.Rev.* **D88** (2013) 064006, [[arXiv:1309.0818](#)], [[doi:10.1103/PhysRevD.88.064006](#)].
 - [45] F. Torsello, M. Kocic, and E. Mortsell, *Classification and asymptotic structure of black holes in bimetric theory*, *Phys. Rev.* **D96** (2017), no. 6 064003, [[arXiv:1703.07787](#)], [[doi:10.1103/PhysRevD.96.064003](#)].
 - [46] P. Breitenlohner, P. Forgacs, and D. Maison, *Gravitating monopole solutions*, *Nucl. Phys. B* **383** (1992) 357–376, [[doi:10.1016/0550-3213\(92\)90682-2](#)].
 - [47] P. Breitenlohner, P. Forgacs, and D. Maison, *Gravitating monopole solutions II*, *Nucl.Phys.B*

- 442** (1994) 126–156, [[gr-qc/9412039](#)].
- [48] P. Breitenlohner, P. Forgacs, and D. Maison, *On Static spherically symmetric solutions of the Einstein Yang-Mills equations*, *Commun. Math. Phys.* **163** (1994) 141–172, [[doi:10.1007/BF02101738](#)].
- [49] S. Hassan and R. A. Rosen, *Confirmation of the secondary constraint and absence of ghost in massive gravity and bimetric gravity*, *JHEP* **1204** (2012) 123, [[arXiv:1111.2070](#)], [[doi:10.1007/JHEP04\(2012\)123](#)].
- [50] S. Alexandrov, *Canonical structure of Tetrad Bimetric Gravity*, *Gen. Rel. Grav.* **46** (2014) 1639, [[arXiv:1308.6586](#)], [[doi:10.1007/s10714-013-1639-1](#)].
- [51] V. O. Soloviev, *Constraint Algebra in Bigravity*, [arXiv:2006.16230](#).
- [52] S. Hassan, A. Schmidt-May, and M. von Strauss, *On Consistent Theories of Massive Spin-2 Fields Coupled to Gravity*, *JHEP* **1305** (2013) 086, [[arXiv:1208.1515](#)], [[doi:10.1007/JHEP05\(2013\)086](#)].
- [53] J. Stoer and R. Bulirsch, *Introduction to numerical analysis*. Springer-Verlag, 1980.
- [54] I. Gelfand, S. Fomin, and R. Silverman, *Calculus of Variations*. Dover Books on Mathematics. Dover Publications, 2000.
- [55] P. Pani, *Advanced Methods in Black-Hole Perturbation Theory*, *Int. J. Mod. Phys. A* **28** (2013) 1340018, [[arXiv:1305.6759](#)], [[doi:10.1142/S0217751X13400186](#)].
- [56] E. Berti, V. Cardoso, and A. O. Starinets, *Quasinormal modes of black holes and black branes*, *Class. Quant. Grav.* **26** (2009) 163001, [[arXiv:0905.2975](#)], [[doi:10.1088/0264-9381/26/16/163001](#)].
- [57] L. Lehner and F. Pretorius, *Final state of Gregory–Laflamme instability*, pp. 44–68. 2012. [arXiv:1106.5184](#).
- [58] M. Kocic, M. Högås, F. Torsello, and E. Mörtzell, *On Birkhoff’s theorem in ghost-free bimetric theory*, [arXiv:1708.07833](#).
- [59] M. Högås, M. Kocic, F. Torsello, and E. Mörtzell, *Generalized Vaidya solutions in bimetric gravity*, [arXiv:1905.09832](#).
- [60] S. W. Hawking and G. F. R. Ellis, *The Large Scale Structure of Space-Time*. Cambridge Monographs on Mathematical Physics. Cambridge University Press, 2011.
- [61] C. Mazuet and M. S. Volkov, *Massive spin-2 field in arbitrary spacetimes – the detailed derivation*, *JCAP* **1807** (2018), no. 07 012, [[arXiv:1804.01970](#)], [[doi:10.1088/1475-7516/2018/07/012](#)].